BBA - Molecular Cell Research 1869 (2022) 119307

Contents lists available at ScienceDirect

BBA - Molecular Cell Research

journal homepage: www.elsevier.com/locate/bbamcr

Research Paper

ISCA2 deficiency leads to heme synthesis defects and impaired erythroid differentiation in K562 cells by indirect ROS-mediated IRP1 activation

Jing Wang [a,1], Mengyao Jiang [a,1], Guanru Yue [b], Lifei Zhu [a], Xueqing Wang [a], Mengxiang Liang [a], Xiaolin Wu [a], Beibei Li [a], Yilin Pang [a], Guoqiang Tan [a,*], Jianghui Li [a,*]

[a] Key Laboratory of Laboratory Medicine, Ministry of Education, Zhejiang Provincial Key Laboratory of Medical Genetics, College of Laboratory Medicine and Life Sciences, Wenzhou Medical University, Wenzhou, China
[b] School of Basic Medical Sciences, Nanchang University, Nanchang, China

ARTICLE INFO

Keywords:
ISCA2
ALAS2
Cell proliferation
Mitochondria
Erythroid differentiation

ABSTRACT

Iron-sulfur (Fe-S) clusters have been shown to play important roles in various cellular physiological process. Iron-sulfur cluster assembly 2 (ISCA2) is a vital component of the [4Fe-4S] cluster assembly machine. Several studies have shown that ISCA2 is highly expressed during erythroid differentiation. However, the role and specific regulatory mechanisms of ISCA2 in erythroid differentiation and erythroid cell growth remain unclear. RNA interference was used to deplete ISCA2 expression in human erythroid leukemia K562 cells. The proliferation, apoptosis, and erythroid differentiation ability of the cells were assessed. We show that knockdown of ISCA2 has profound effects on [4Fe-4S] cluster formation, diminishing mitochondrial respiratory chain complexes, leading to reactive oxygen species (ROS) accumulation and mitochondrial damage, inhibiting cell proliferation. Excessive ROS can inhibit the activity of cytoplasmic aconitase (ACO1) and promote ACO1, a bifunctional protein, to perform its iron-regulating protein 1(IRP1) function, thus inhibiting the expression of 5′-aminolevulinate synthase 2 (ALAS2), which is a key enzyme in heme synthesis. Deficiency of ISCA2 results in the accumulation of iron divalent. In addition, the combination of excessive ferrous iron and ROS may lead to damage of the ACO1 cluster and higher IRP1 function. In brief, ISCA2 deficiency inhibits heme synthesis and erythroid differentiation by double indirect downregulation of ALAS2 expression. We conclude that ISCA2 is essential for normal functioning of mitochondria, and is necessary for erythroid differentiation and cell proliferation.

1. Introduction

The earliest studies of iron-sulfur clusters began in the 1960s with the discovery of electron paramagnetic resonance (EPR) signals in purified proteins [1]. Iron-sulfur cluster, an ancient protein inorganic cofactor, plays an indispensable role in various cellular physiological processes [2]. Iron-sulfur protein is involved in the proper functioning of a living cell, from electron transfer in the mitochondrial respiratory chain to catalysis of biochemical reactions, and from the maintenance of genomic stability to the regulation of gene expression. Therefore, intracellular iron-sulfur protein synthesis is essential for normal cell metabolism [3,4]. Many studies have shown that the iron-sulfur cluster assembly (ISC) system is highly conserved from yeast to human cells [5,6]. Type A proteins in the ISC assembly system play an important role in the biogenesis of [4Fe-4S] protein. Two type A proteins, Isa1 and Isa2, were found in eukaryotic yeast and are homologous to ISCA1 and ISCA2 in human cells [7].

In human cells, the biogenesis of iron-sulfur clusters is mostly accomplished in mitochondria by the ISC system, and can be summarized in three steps. First, the [2Fe-2S] cluster is synthesized de novo on the mitochondrial ISCU protein. Second, it is released from the ISCU and bound to the transporters through chaperone proteins. Finally, the proteins are assembled into mature iron-sulfur clusters specifically bound to the target protein in the mitochondria. This process is accompanied by the synthesis of [4Fe-4S] protein [6]. In Hela cells, ISCA2 deficiency has been shown to result in decreased activity of mitochondrial cis-aconitase (ACO2) and complex I. ISCA2 deficiency has also been shown to result in a decrease in mitochondrial [4Fe-4S]

* Corresponding authors.
E-mail addresses: tgq@wmu.edu.cn (G. Tan), lijianghui1980@126.com (J. Li).
[1] These authors have contributed equally to this work.

https://doi.org/10.1016/j.bbamcr.2022.119307
Received 28 November 2021; Received in revised form 30 May 2022; Accepted 8 June 2022
Available online 14 June 2022

protein expression, but does not affect mitochondrial [2Fe-2S] protein and cytoplasmic [4Fe-4S] protein expression. Interestingly, ACO1 activity decreases due to low ISCA2 expression [7]. ISCA2 is not required for the synthesis of [4Fe-4S] protein in mouse primary neurons and skeletal muscle cells [8]. Point mutations in ISCA2 induce multiple mitochondrial dysfunction syndrome 4 (MMDS4), which is defective in the same metabolic pathway as other MMDSs [9]. The ISCA2 G77S mutation causing leukoencephalopathy was first reported in a paper published in 2015 [10], and 10 patients have been found in whom the disease is caused by a faulty ISCA2 gene. In 2017, researchers detected ISCA2 c.229GS > A mutation in patients; GLy77Ser cells also confirmed the role of ISCA2 in [4Fe-4S] protein synthesis [11].

Interestingly, several articles have consistently proposed that ISCA2 is highly expressed during human erythrocyte differentiation. A large-scale gene-screening analysis revealed strong co-expression between heme biosynthesis and the Fe-S cluster assembly proteins ISCA1, ISCA2, and IBA57 [12–14]. Nilsson's paper also points out that when heme synthase is overexpressed, ISCA1 and ISCA2 will enhance their expression in parallel [14]. Subsequent studies used zebrafish embryos for in situ hybridization experiments. The results showed that ISCA1 and IBA57 were specifically expressed in zebrafish embryos, and that defects of both led to anemia in zebrafish, with a reduction in the expression levels of heme and hemoglobin [14]. Three cofactors, ISCA1, ISCA2 and IBA57, interact with each other, and deletion of any of the protein coding genes can lead to similar phenotypes [7,15,16]. However, an ISCA2 knockdown assay in HeLa cells found no significant change in heme content after ISCA2 expression reduction; thus, it was concluded that ISCA2 is not necessarily related to heme synthesis [7], contradicting previous research. Additionally, it is worth noting that Hela cells, as non-erythroid cells, have low intracellular heme content. If ISCA2 knockout is conducted in erythroid cells, the relationship between ISCA2 and heme synthesis will be better reflected. Previous studies on ISCA2 have mainly focused on the role of this gene in the assembly of Fe-S clusters, but have not examined the influence of mitochondrial function on the cell itself. To better understand the effect of ISCA2 on mitochondrial function and the cell, and to further explore whether ISCA2 affects heme synthesis and hemoglobin, human erythroid leukemia cell K562 cells were selected. We used RNAi technology to knock down intracellular ISCA2, and designed cells with ISCA2 overexpression as controls. Mitochondrial function, biogenesis, and morphology were measured, and cell behaviors, such as proliferation and the ability to differentiate into erythrocytes, were detected in an attempt to elucidate the underlying mechanisms. We found that ISCA2 deficiency indeed causes mitochondrial dysfunction, inhibiting cell proliferation and erythroid differentiation. This discovery provides us with a more complete understanding of the function of the ISCA2 and provides a new direction for the study of anemia.

2. Results

2.1. ISCA2 knockdown repressed the proliferation of K562 cells

ISCA2 stable knockdown cells were generated through the lentivirus transduction by two separate short hairpin RNA sequences. Western blot (WB) and quantitative real-time polymerase chain reaction (qPCR) were used to detect ISCA2 expression. As expected, qPCR and WB were performed to confirm the knockdown of ISCA2 (Fig. 1A, B). During the maintenance of the cell lines, we found that ISCA2 knockdown cells grew more slowly than control cells. To verify this, cell proliferation was measured using viable cell counting assay and the CCK8 assay. The results showed that ISCA2 knockdown (sh-ISCA2-1, sh-ISCA2-2) in K562 cells decreased cell proliferation compared to the control (Fig. 1C, D). Moreover, clonogenic assays demonstrated that the clone formation abilities were also attenuated upon ISCA2 depletion (Fig. 1E, F). To further determine whether the decreased cell proliferation was affected by the cell cycle distribution, the cell cycle distribution was determined by flow cytometry analysis. The results indicated that knockdown of ISCA2 induced G2/M phase arrest in K562 cells (Fig. 1G, H, I). To further verify the effects of ISCA2 on cell proliferation, we replaced the high glucose medium with galactose medium before performing a CCK8 assay. Interestingly, cell proliferation ceased and the cell number was reduced after growing for 72 h. Nevertheless, cells with low expression of ISCA2 showed a slower proliferation rate than control cells before 72 h (Fig. 1J). Collectively, these data demonstrate that ISCA2 plays a vital role in the regulation of cell proliferation.

2.2. ISCA2 knockdown is expected to result in decreased oxidative phosphorylation (OXPHOS) and impaired mitochondrial respiratory efficiency

As the integrity of the mitochondrial respiratory chain complexes is important for normal cellular aerobic respiration and OXPHOS, we investigated the effects of ISCA2 deletion on mitochondrial respiration and oxidative phosphorylation. We measured the protein expression level of unstable subunits from each of the five mitochondrial respiratory complexes. We found that protein expression of the subunits of complex I and II with [4Fe-4S] clusters decreased, such as NDUFS1, NDUFS8, SDHA, and SDHB, but only in the case of extreme depletion of ISCA2. The protein expression levels of COX IV and ATP5a, without any form of iron-sulfur cluster, unstable subunits of the respiratory chain complexes IV and V, were unaffected by ISCA2 deficiency. Interestingly, the expression of UQCRFS1 and UQCRB of the subunit of complex III, with only [2Fe-2S] as the active center, decreased after ISCA2 deficiency (Fig. 2A, B). The mitochondrial oxygen consumption rate (OCR) was measured by an extracellular flux analyzer to reflect the main function of mitochondrial energy respiration. As shown in Fig. 2C, down-regulation of ISCA2 significantly reduced mitochondrial OCR. In the Seahorse experiment, maximum or basic respiration indicated a significant decline in mitochondrial respiratory flux and spare respiration exhibited a compensatory increase, suggesting that ISCA2 knockdown blocked OXPHOS (Fig. 2D, G, F). Additionally, ATP production was calculated, and significant ATP loss, which did not meet the cellular ATP requirements that support cell growth, was shown in ISCA2 knockout cells (Fig. 2E). Overall, mitochondrial OCR testing with the Seahorse XF96 analyzer revealed an important link between ISCA2 and OXPHOS.

2.3. ISCA2 overexpression is beneficial to mitochondrial aerobic respiration

To verify whether ISCA2 deficiency affected the proliferation of K562 cells by regulating OXPHOS, we designed and synthesized the ISCA2 overexpression plasmid. We overexpressed the ISCA2 gene by lentiviral transfection in wild type K562 cells. And we used qPCR and immunoblotting to determine the high expression of ISCA2 (Fig. 3A, B). These results indicated successful construction of the K562 cell model of ISCA2 gene overexpression. In ISCA2 overexpressed cells, we found that protein expression of the subunits of complex I and II slightly increased. The protein expression levels of COX IV and ATP5a were unaffected by ISCA2 expression. The expression of UQCRFS1 and UQCRB increased (Fig. 3C, D). To further investigate whether ISCA2 deficiency impaired energy metabolism by damaging the respiratory chain complexes, we first measured cellular ATP and L-lactic acid production. As shown in Fig. 3E, compared to the control group, when ISCA2 expression was inhibited, intracellular relative ATP production decreased significantly, but ATP production increased in the ISCA2 overexpressed cells (Fig. 3E). When intracellular ISCA2 was reduced, L-lactic acid production increased greatly, and intracellular L-lactic acid content showed an obvious downward trend after ISCA2 overexpression (Fig. 3F).

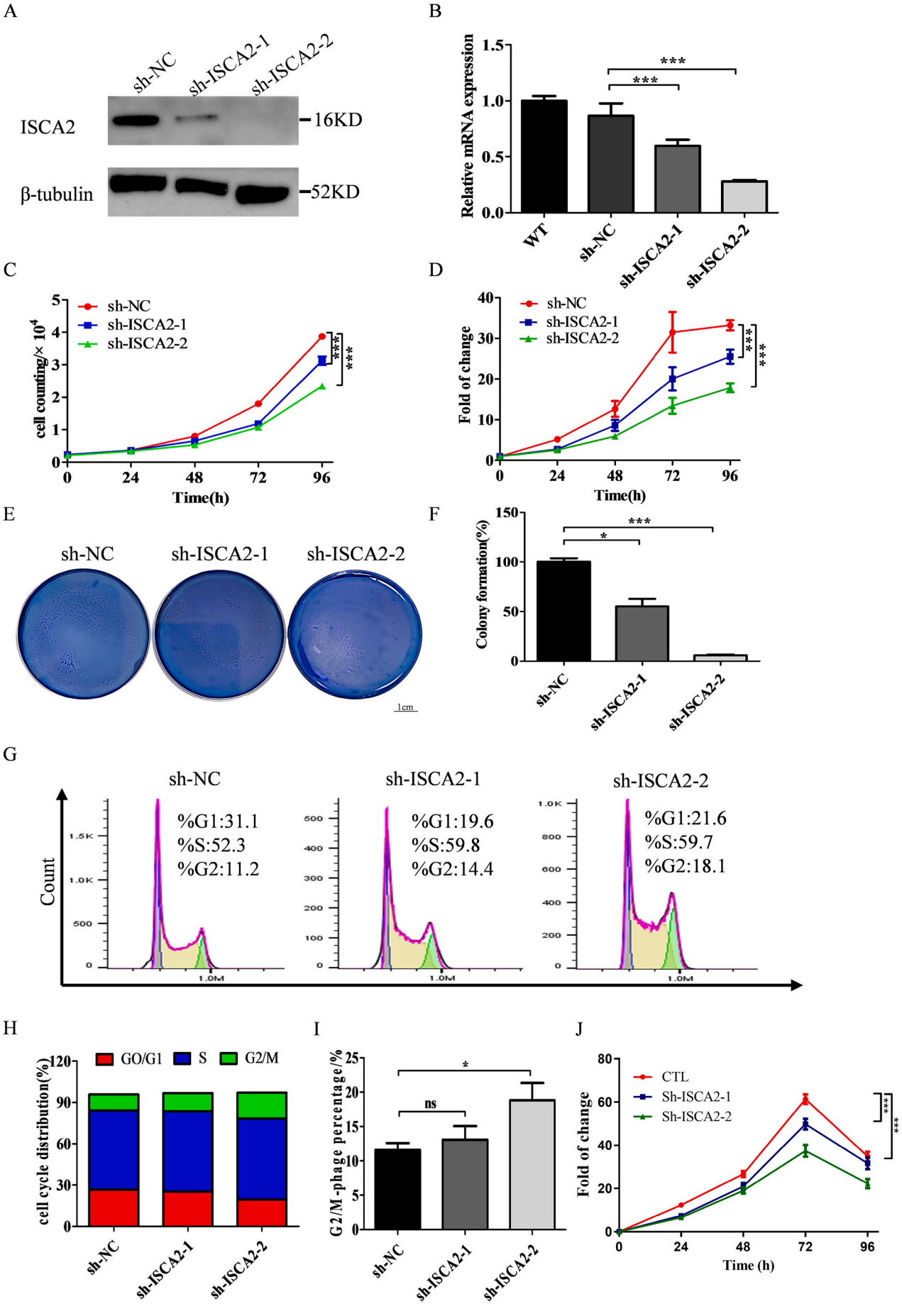

(caption on next page)

Fig. 1. ISCA2 knockdown repressed the proliferation of K562 cells. (A) Western blot analysis protein expression level of ISCA2 knockdown and control K562 cells. (B) Quantitative real-time PCR of ISCA2 mRNA in the three indicated K562 cells. (C) Viable cell count growth curves. (D) The proliferation of control and sh-ISCA2 cells was detected by CCK8 assay. (E-F) Effects of ISCA2 suppression in K562 cells on the proliferation capacity were measured by plate clone formation assay. (G) Flow cytometric analysis of the cell cycle in stable K562 cell lines. (H-I) The percentage of cells in the various phases of the cell cycle was estimated by flow cytometric analysis. (J) Growth curves of K562 cells in galactose medium. Images are representative of three independent experiments. Asterisks indicate that the differences between samples were statistically significant according to an independent-sample *t*-test, $*p < 0.05$, $**p < 0.01$. $***p < 0.001$.

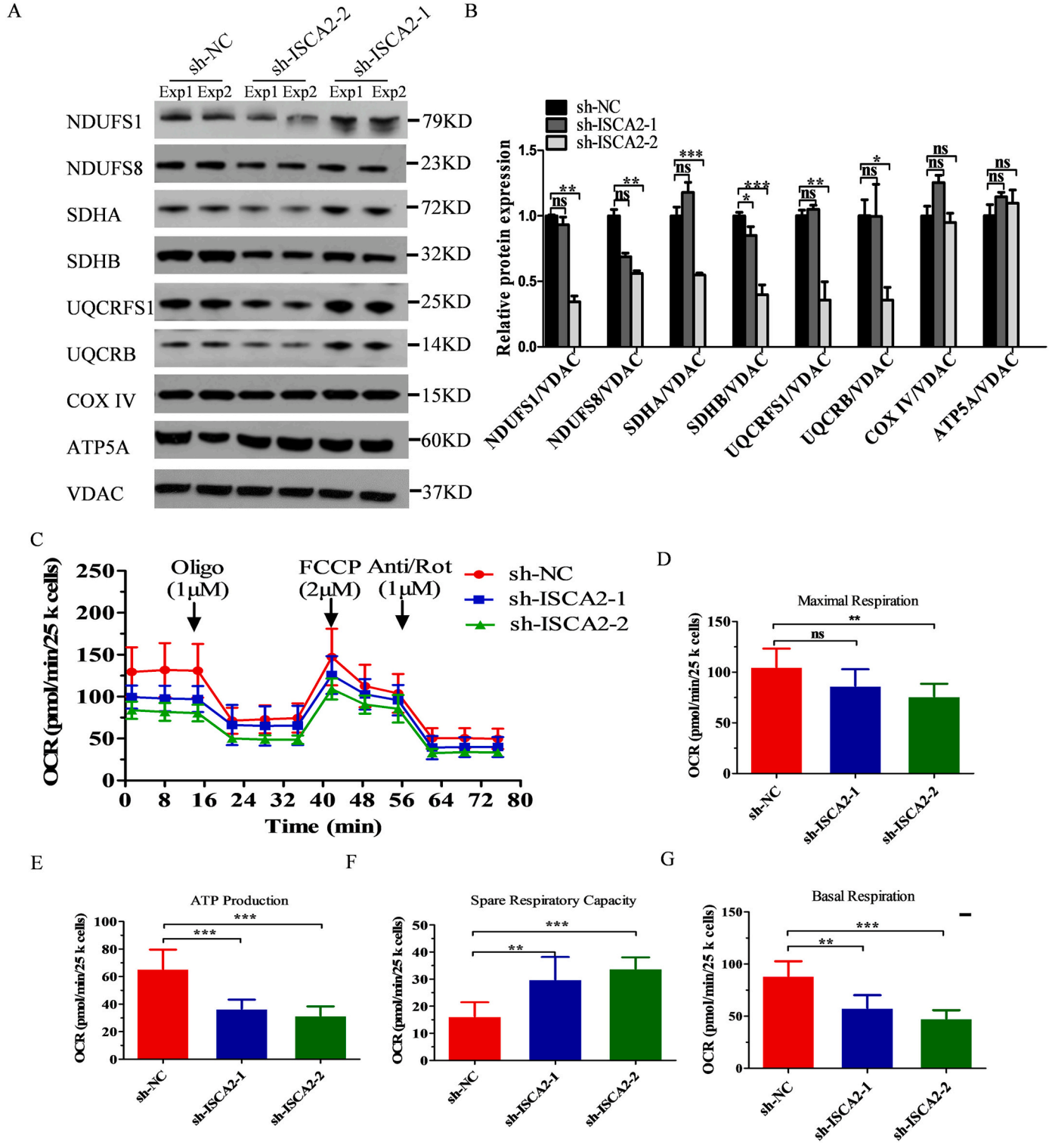

Fig. 2. ISCA2 knockdown is expected to result in decreased OXPHOS and impaired mitochondrial respiratory efficiency. (A) Immunoblot showing the levels of labile subunits from each of the five mitochondrial respiratory complexes in K562 (ISCA2 knockdown/sh-NC) cells. (B) The relative protein expression levels of unstable subunits from each of the five mitochondrial respiratory complexes were quantified according to the protein gray values. (C) The OCR rate was calculated by an extracellular flux analyzer following addition of oligomycin, FCCP, and antimycin A. (D-G) The basal respiration, maximal respiration, spare respiration, and ATP production were calculated. Images are representative of three independent experiments. Asterisks indicate that the differences between samples were statistically significant according to an independent-sample *t*-test, $*p < 0.05$, $**p < 0.01$. $***p < 0.001$.

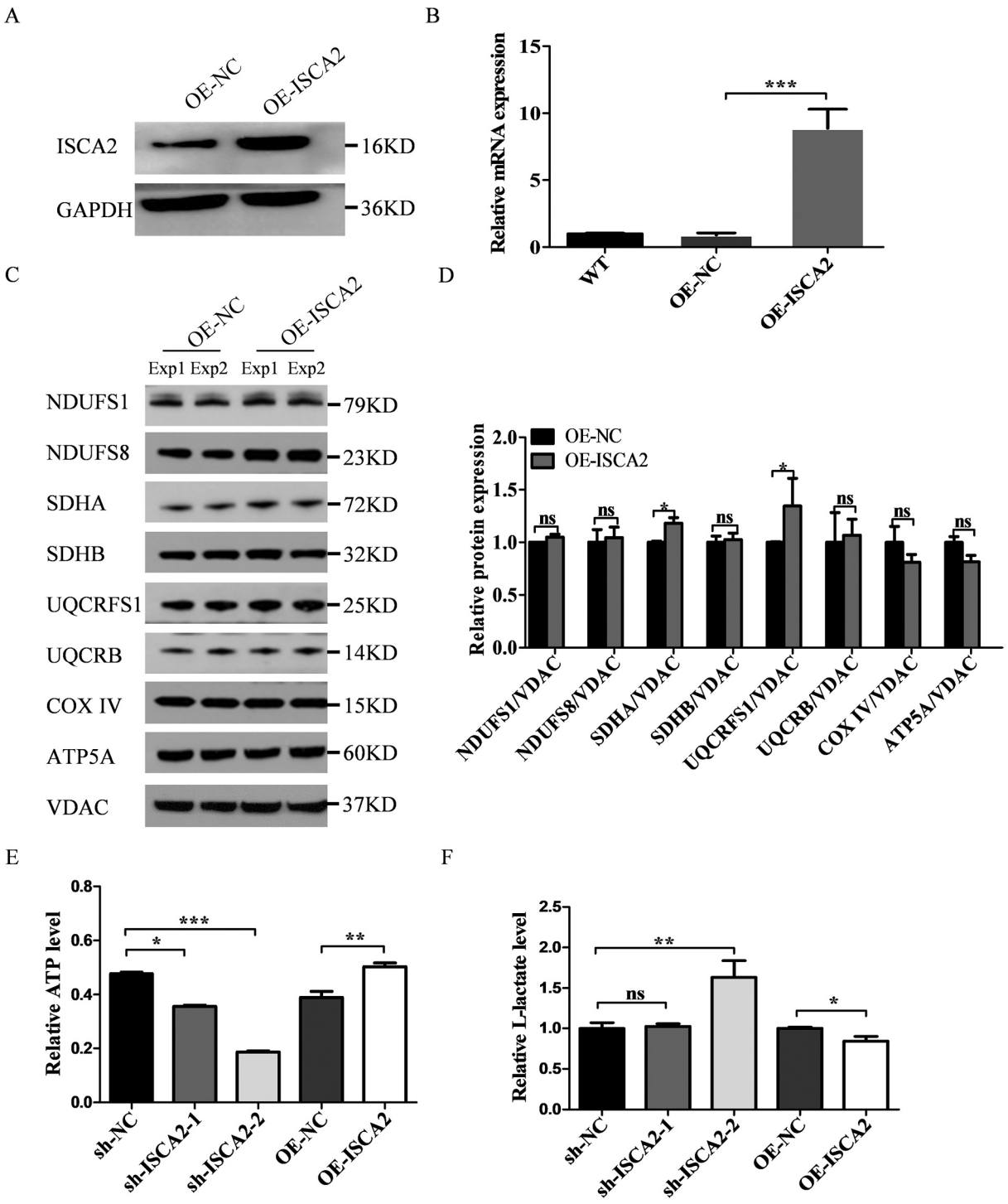

Fig. 3. ISCA2 overexpression is beneficial to mitochondrial aerobic respiration. (A) Immunoblot analysis protein expression level of ISCA2 overexpression and control K562 cells. (B) QPCR of ISCA2 mRNA in the two indicated K562 cells. (C) Immunoblot showing the levels of labile subunits from each of the five mitochondrial respiratory complexes in K562 (OE-ISCA2/OE-NC) cells. (D) The relative protein expression levels of unstable subunits from each of the five mitochondrial respiratory complexes were quantified according to the protein gray values. (E) Relative ATP levels indicated by protein content. (F) Relative L-lactate levels revised by protein content. Images are representative of three independent experiments. Asterisks indicate that the differences between samples were statistically significant according to an independent-sample *t*-test, $*p < 0.05$, $**p < 0.01$. $***p < 0.001$.

2.4. Elevated expression of ISCA2 in wild type K562 cells promotes their proliferation

We plotted the growth curves of the two groups of cells using cell counting and CCK8 methods. As expected, the cell proliferation ability of the group of OE-ISCA2 was higher than that of controls (Figs. 4A, B). We obtained comparable results in the clone formation experiment. The results showed that the number of clones increased when ISCA2 was overexpressed, demonstrating that overexpression of ISCA2 facilitated the amplification of K562 cells (Fig. 4C, D). We measured the cell cycle of ISCA2 overexpressing cells by flow cytometry. Unlike the previous group of ISCA2 knockout cells, high expression of ISCA2 promoted the

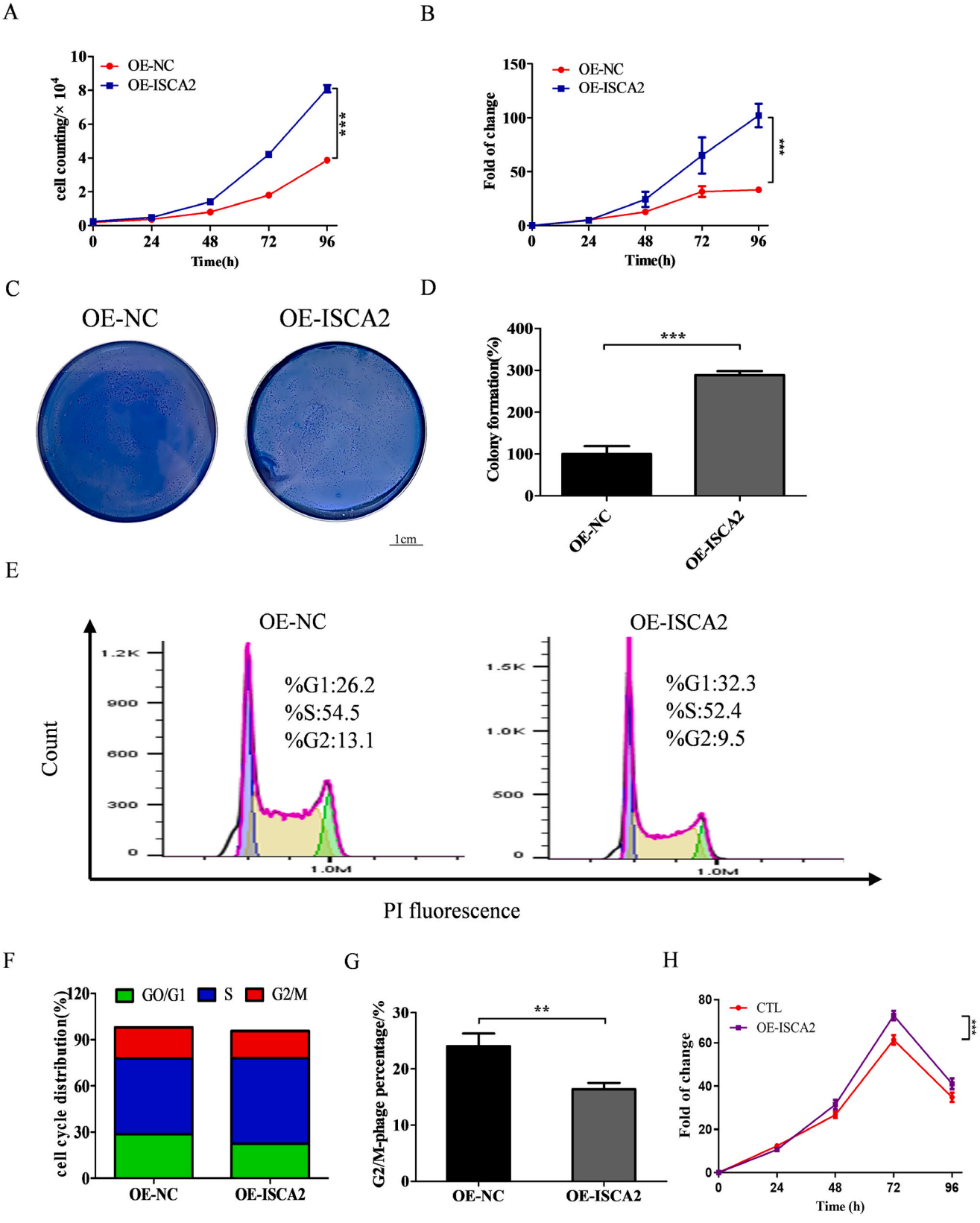

Fig. 4. Elevated expression of ISCA2 in K562 cells promotes their proliferation. (A) Cell-counting experiments showed that overexpression of ISCA2 significantly accelerates cell proliferation. (B) CCK8 assay demonstrated that high expression of ISCA2 promotes cell viability. (C-D) The clone formation capacity of K562 cells was evaluated by clone formation assays. (E) Cell cycle was measured by flow cytometry. (F-G) Histogram indicating the distribution of K562 cells in each stage of the cell cycle. (H) Growth curves are drawn in galactose medium but not in glucose medium. Images are representative of three independent experiments. Asterisks indicate that the differences between samples were statistically significant according to an independent sample *t*-test, $^{*}p < 0.05$, $^{**}p < 0.01$. $^{***}p < 0.001$.

cell cycle transition from G2/M to G0/G1 phase (Fig. 4E, F, G). In contrast to ISCA2 knockdown cells, cells with high expression of ISCA2 displayed a conspicuously faster proliferation speed than control cells before 72 h, although they all died gradually thereafter (Fig. 4H). ISCA2 can be regarded as one of the main factors affecting the proliferation of K562 cells.

2.5. Reduction of ISCA2 indirectly leads to the accumulation of ROS, the destruction of mitochondrial morphology, and the inhibition of mitochondrial biogenesis

To further explore the effect of ISCA2 deficiency on mitochondrial biogenesis, we first determined the mitochondrial DNA (mtDNA) copy number as a parameter of mitochondrial function. As shown in Fig. 5A, when the expression of ISCA2 was overly decreased, the copy number of mtDNA also displayed a distinct declining trend. Moreover, the copy number of mtDNA increased significantly following overexpression of ISCA2. Second, mitochondria were labeled with the MitoTracker deep red probe and monitored using an automatic microplate reader. The results also showed that ISCA2 deficiency decreased the number of viable mitochondria in the cell, whereas high ISCA2 expression promoted a slight increase in the number of mitochondria (Fig. 5B). Production of ROS is a normal part of the electron transport chain (ETC) in the mitochondria, and impairment of ETC promotes ROS production [17]. To investigate whether ISCA2 deficiency indirectly leads to ROS accumulation by disrupting ETC, we further detected ROS content in mitochondria. We discovered that ISCA2 defect produced the accumulation of ROS, suggesting that the cells were under oxidative stress. However, the ETC of ISCA2 overexpressed cells were not damaged, so ROS content did not increase. (Fig. 5C). The NAD^+/NADH ratio is a critical indicator that reflects the REDOX state of cells, and can therefore be used to determine the metabolic activity and health of a cell. We measured the relative contents of NAD^+ and NADH in cells using a colorimetric method and calculated their ratios. Compared to the control group, the ratio of NAD^+/NADH decreased in cells with low ISCA2 expression, while the ratio of NAD^+/NADH increased significantly after high expression of ISCA2 (Fig. 5D). This finding further suggests that ISCA2 deficiency causes mitochondrial dysfunction. In order to more intuitively observe the significance of ISCA2 in maintaining normal mitochondrial function, the intracellular mitochondria were observed by transmission electron microscopy. The results showed large inclusions, which represented heavily enlarged mitochondria in ISCA2 defective cells. Moreover, some of the mitochondrial cristae were decreased, and the density decreased or was even vacuolated. The mitochondrial morphology of ISCA2 overexpressing cells was normal, consistent with that of the control group (Fig. 5E).

2.6. ISCA2 promotes cell proliferation and inhibits apoptosis by regulating ROS production

Preliminary results showed that ISCA2 knockdown destroys mitochondrial OXPHOS and indirectly induces ROS production. We suspected that ROS production would lead to cell apoptosis, which may also explain the slower cell proliferation. Therefore, we tested the cell apoptosis rate of ISCA2 deficient cell lines and ISCA2-overexpressing cell lines, and the results are shown in Fig. 6A, B, C. ISCA2 knockdown led to an increased apoptosis rate. To determine whether the slowing of cell proliferation was affected by excessive ROS, 5 mM antioxidant N-Acetyl-L-cysteine (NAC) was added to the culture medium to treat cells to reduce ROS [18], and the intracellular ROS level was measured. As expected, NAC effectively reduced intracellular ROS (Fig. 6D). The cell viability and proliferation were further measured. We found that when ROS in ISCA2-deficient cells was reduced, cell proliferation was significantly stronger than that in cells expressing low levels of ISCA2, but it did not recover to the level of the control group (Fig. 6E–G). We believe that ISCA2 influences cell proliferation by regulating OXPHOS and ROS production.

2.7. Depletion of ISCA2 exerts complex effects on intracellular iron and indirectly leads to decreased ACO1 activity to further play the IRP1 function by non-directly regulation of ROS

In previous study, researchers proposed evidence that both *Escherichia coli* IscA and the homologous protein of IscA, human ISCA1 protein, bind iron and Fe-S clusters [19–21]. Therefore, we investigated whether ISCA2, a homolog of ISCA1, affects iron metabolism. We performed WB detection of proteins associated with intracellular iron metabolism. We found a slight increase in ferritin receptor (TFR1) expression and a significant decrease in ferritin and ferritin light chain (FTL) expression in ISCA2-deficient cells. When the expression of ISCA2 was enhanced, the expression of TFR1 decreased noticeably, and the expression of ferritin and FTL increased slightly. The protein expression levels of iron regulatory protein 2 (IREB2) increased slightly with the decrease in ISCA2 expression, but decreased in ISCA2 overexpressing cells (Fig. 7A). It is not surprising that ISCA2 knock-down leads to increased TfR1 and decreased ferritin heavy chain mRNA levels (Fig. 7B). To determine whether these effects of ISCA2 knockdown on iron regulatory proteins were sufficient to affect cellular iron, we measured the labile iron pool (LIP), a measure of cytosolic free iron. The results showed that there was a negative correlation between intracellular LIP content and ISCA2 expression (Fig. 7C, D). Next, we determined the activities of mitochondrial and cytoplasmic aconitase, important [4Fe-4S] proteins that catalyze the reaction from citric acid to isocitrate, using an in-gel activity assay. The breakdown of mitochondrial protein ISCA2 resulted in a more dramatic decrease in cytoplasmic aconitase activity than mitochondrial aconitase activity, though without obvious changes in protein level (Fig. 7E). When the Fe-S cluster of cytosolic aconitase is destroyed, it not only loses aconitase activity but also gains a new function: the ability to bind to iron regulatory elements (IREs) in protein mRNA, which regulate iron transport and storage. This conformation of c-aconitase and IRE is called IRP1. We found that IRP1 activity increased when ACO1 activity was decreased in ISCA2 deficient cells. IRP1 activity did not increase when ACO1 activity was increased in ISCA2 overexpressed cells (Fig. 7E–G). To further explore why ISCA2 affects the activity of c-aconitase, we treated ISCA2 deficient cells with NAC and Defetoxamine (DFO). Previous data have shown that cells treated with 5 mM of NAC for 2 h had significantly reduced ROS levels. We treated cells with 100 mM DFO for 48 h and found that the ISCA2 knockdown group had the same iron divalent level as the control group (Fig. 7H). We measured the activity of ACO1 in each group again and found that adding NAC reduced the intracellular ROS level and adding DFO reduced the cytoplasmic free iron level, both of which promotes the recovery of ACO1 activity (Fig. 7I, J).

2.8. ISCA2 expression can affect the expression of ALAS2 and thus altering heme synthesis, which may be related to the indirect regulation of ACO1/IRP1 activity by ISCA2

Our previous data suggest that ISCA2 deficiency inhibits the Fe-S cluster binding activity of ACO1 through ROS and accumulation of iron, promoting its IRP1 function. IRP1 binds to IREs of ALAS2 and inhibits its translation. As expected, a reduction in heme content was observed in ISCA2-deficient cells. Compared to the control group, the intracellular heme content of ISCA2 overexpressing cells was significantly increased (Fig. 8A, B). Given that the initial and final stages of heme synthesis are conducted in mitochondria, and these two steps each contain a key enzyme that regulates heme synthesis, we detected the content of these enzymes by western blot. The first enzyme that regulates heme synthesis is ALAS2, and an important enzyme called ferrochelase (FECH) is also required in the last step of heme synthesis. Our results showed that when ISCA2 was deficient, the expression of ALAS2 was decreased, but FECH was unaffected. The expression of ALAS2 was

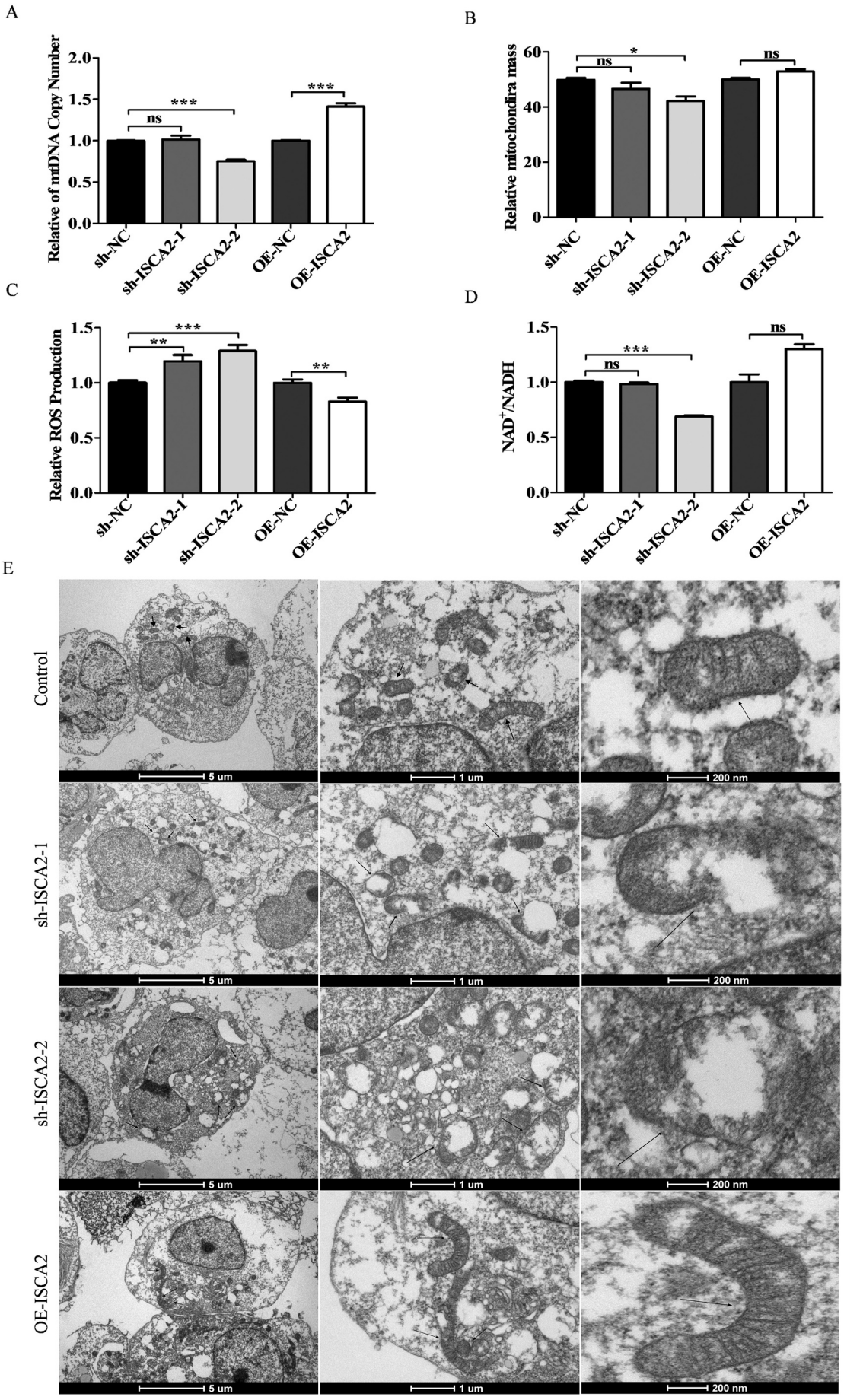

(caption on next page)

Fig. 5. Reduction in ISCA2 leads to the accumulation of ROS and the destruction of mitochondrial morphology, which seriously inhibits mitochondrial biogenesis. (A) Mitochondrial DNA copy number was tested by qPCR-based assay. (B) Mitochondrial biogenesis was detected by Mito-Tracker Deep Red staining, and flow cytometry was used to measure the number of living mitochondria bound to Mito-Tracker. (C) Mitochondrial ROS levels were determined using Mito-SOXTM Red mitochondrial superoxide indicator. (D) NAD^+ and NADH levels were measured, and the NAD^+/NADH rate was counted. (E) The visual morphological changes of mitochondria were observed by transmission electron microscopy (TEM). Images are representative of three independent experiments. Asterisks indicate that the differences between samples were statistically significant according to an independent sample *t*-test, $*p < 0.05$, $**p < 0.01$. $***p < 0.001$.

slightly increased in ISCA2 overexpressing cells, while FECH was not significantly changed (Fig. 8C–F). QPCR results showed that the ISCA2 deficiency restrained the transcription of ALAS2 at the mRNA level, and we also observed downregulation of GATA1. The high expression of ISCA2 promoted the transcription of ALAS2, but had no overt effect on GATA1 (Fig. 8G, H). In other words, in erythroid cells, the low expression of ISCA2 is detrimental to heme synthesis by inhibiting the expression of ALAS2, while the overexpression of ISCA2 is beneficial to the expression of ALAS2, thus promoting heme synthesis.

2.9. ISCA2 knockdown repressed the erythroid differentiation of K562 cells, which was rescued by overexpression of ISCA2

K562, the erythroleukemia cell line, can differentiate into erythrocytes under hemin induction, mainly expressing α-globin, ε-globin, and γ-globin, and can detect the increased expression of cd235a. Benzidine staining can determine the degree of erythroid differentiation. Hemin was added to induce the cells to differentiate into erythrocytes. We first explored the conditions that successfully led to erythroid differentiation in wild-type K562 cells. To this end, the cells were divided into two groups: The first group was induced with 30 μM hemin for 0 h, 24 h, 48 h, and 72 h, and the second group was induced with the same amount of hemin for the same time. The difference in the second group of cells was that hemin was removed after induction for 24 h. The cells were then tested by qPCR and stained with benzidine. The results of qPCR showed that the mRNA expression of γ-globin and cd235a were increased following treatment with 30 μM hemin for 24 h, 48 h, and 72 h. However, when hemin was removed after induction for 24 h, and the cells were further cultured for 48 h or 72 h, the mRNA expression of γ-globin and cd235a was not significantly increased (Fig. 9B, C). The results of benzidine staining showed that hemin induced hemoglobin expression in cells after 24 h (Fig. 9A). Therefore, it can be concluded that cells treated with 30 μM hemin for 24 h can successfully induce erythroid differentiation. Subsequently, hemin was added to the medium of ISCA2 underexpressing or overexpressing cells for induction, and the expression levels of genes related to erythroid differentiation, such as γ-globin, cd235a, HBG1, HBG2, were detected by qPCR (Fig. 9G–J). We found that the expression level of ISCA2 was positively correlated with the expression level of genes related to erythroid differentiation in cells. Benzidine staining also showed that cells with low ISCA2 expression had a low positive staining rate, and that cells with a high ISCA2 expression level had more positive cells (Fig. 9D, E). We next used the hemoglobin detection kit to more accurately quantify the intracellular hemoglobin level. Consistent with the results of benzidine staining, when intracellular ISCA2 expression decreased, the relative heme content also decreased, and the intracellular relative heme content increased with high ISCA2 expression (Fig. 9K, L). To further substantiate the argument, we tested fetal hemoglobin (HBF) in cells by western blotting, which also showed low HBF expression in an ISCA2 deficient cell line and high HBF expression in ISCA2 high-expressing cells (Fig. 9F). Taken together, these results suggest that ISCA2 deficiency can block the erythroid differentiation of K562 cells.

2.10. ISCA2 could promote or inhibit intracellular heme synthesis and erythroid differentiation by doubly and indirectly regulating the expression of ALAS2

Our results indicate that ISCA2 deficiency is detrimental to the expression of ALAS2. We sought to determine whether this was because the low expression of ALAS2 inhibits the erythroid differentiation. To investigate this, we overexpressed the ALAS2 gene in ISCA2-deficient cells. We obtained a stable K562 cell line with high ALAS2 expression but low ISCA2 expression (Fig. 10A, B). Then, we induced the constructed cell lines according to the previous method, and collected the cells after 24 h for use in qPCR to verify the expression of genes related to erythroid lineage differentiation. QPCR results showed that after ALAS2 was highly expressed in ISCA2 low expression cell lines, compared to the ISCA2 low expression group, the expression levels of erythroid differentiation-related indicator genes showed an increased trend, and even reached or exceeded the expression levels of the control group (Fig. 10E, F). We also quantified the relative intracellular hemoglobin content, and the results were consistent with our expectations. Following overexpression of ALAS2, the intracellular hemoglobin content returned to the level of the previous control group, but was higher than the level of hemoglobin in ISCA2-deficient cells (Fig. 10C). To determine whether overexpression of ALAS2 can rescue heme synthesis, we measured the heme content in uninduced cells. We found that the recovery of ALAS2 was indeed beneficial to heme synthesis in ISCA2-deficient cells (Fig. 10D). Previous data suggest that ISCA2 deficiency indirectly leads to the accumulation of ROS, which further inhibits the activity of ACO1 and acts as an activator of IRP1 activity. To determine whether increased IRP1 activity can inhibit ALAS2 translation by binding to the IRE fragment of the 5 ‘UTR of ALAS2, we designed an IRE-containing ALAS2 overexpressed plasmid and transfected it into ISCA2-deficient cells. We next detected ALAS2 protein expression level and relative heme content. Our previous data suggest that transfection of IRE-lacking ALAS2 into ISCA2-deficient cells can rescue ALAS2 protein expression. However, expectedly, when we transfected IRE-containing ALAS2, the expression of ALAS2 in ISCA2-deficient cells was still low. Of course, the relative heme content was significantly lower than ISCA2-deficient cells transfected with ALAS2 without IRE (Fig. 10G–I). The results of the ALAS2 recovery assay showed that ISCA2 could indeed promote or inhibit intracellular heme synthesis and erythroid differentiation of K562 cells by doubly and indirectly regulating the expression of ALAS2.

3. Discussion

Our study investigated the effects of ISCA2 on cell proliferation, mitochondrial homeostasis, intracellular heme synthesis, erythroid differentiation and intracellular iron metabolism. We have illustrated these effects and their specific mechanisms through the following two diagrams (Figs. 11, 12). Fig. 11 demonstrating vividly the mechanism by which ISCA2 inhibits cell proliferation and erythroid differentiation. Specifically, ISCA2 deficiency is detrimental to the expression of respiratory chain complex I, II and III subunit proteins, thereby affecting mitochondrial OXPHOS, resulting in a decrease in ATP, and indirectly leading to an increase in ROS. The reduced ATP cannot meet the normal proliferation needs of K562 cells, and the accumulated ROS also inhibits the proliferation of K562 cells to a certain extent. The ISCA2 defect produces a lot of ferrous ions, which may be associated with increased transferrin expression and decreased ferritin expression. The combination of excessive ferrous iron and ROS may lead to damage of the ACO1 cluster and higher IRP1 function. IRP1 can bind to the IRE fragment on the 5 ‘UTR of ALAS2, thereby inhibiting its translation, resulting in reduced heme synthesis and reduced erythroid differentiation. Fig. 12

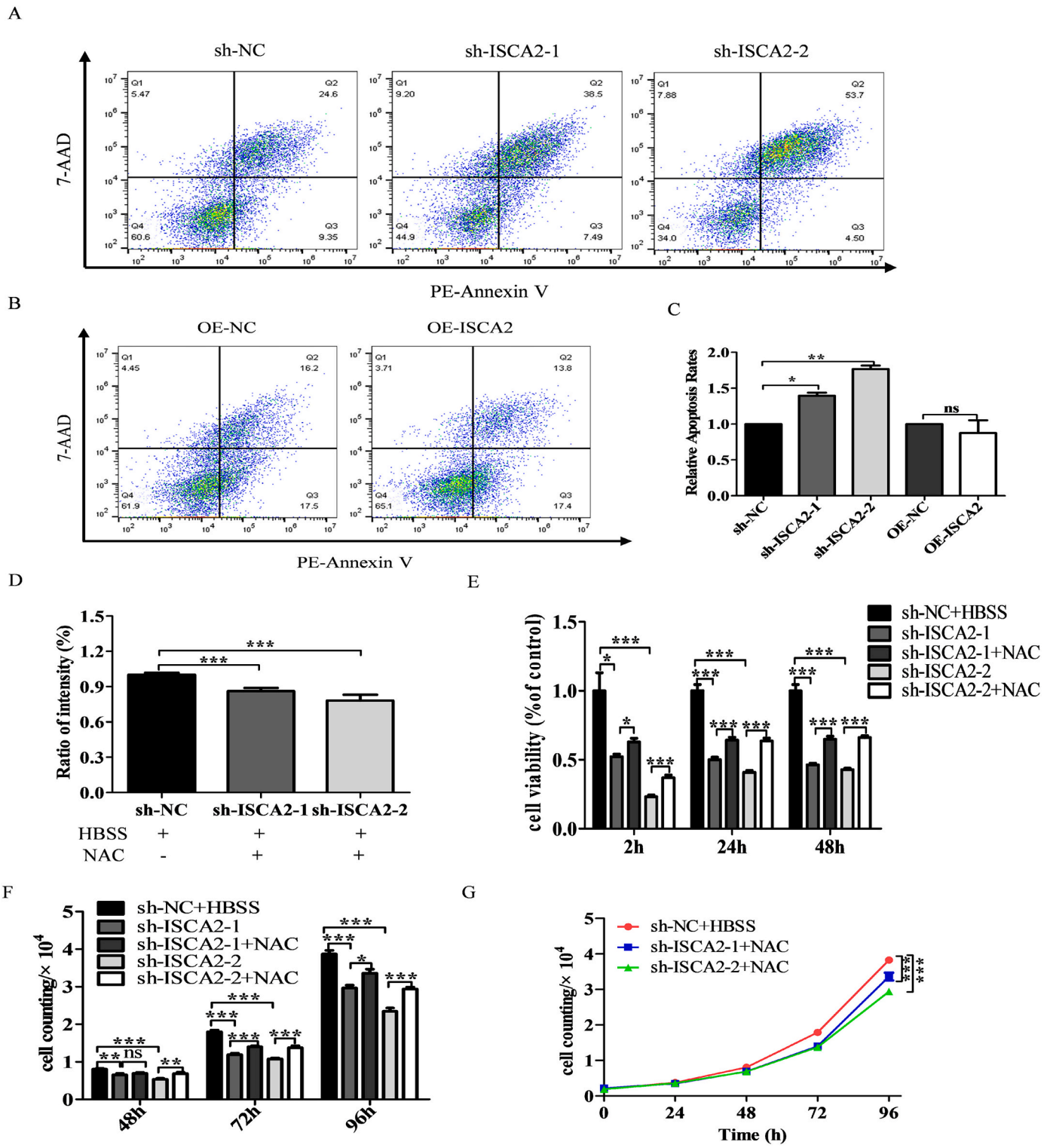

Fig. 6. ISCA2 promotes cell proliferation and inhibits apoptosis by regulating ROS production. (A-B) Apoptosis assay by flow cytometric analysis. (C) The ISCA2 cell apoptotic rate statistically depicted in columns. (D) ROS relative production was estimated by ROS assay. (E) Cell viability was measured by CCK8 kit. (F) Cell proliferation analysis showed a significant difference in the K562 cell proliferation between the NAC intervention group and the ISCA2 knockdown group and control group. (G) Proliferation was measured by cell counts. Images are representative of three independent experiments. Asterisks indicate that the differences between samples were statistically significant according to an independent sample *t*-test, $*p < 0.05$, $**p < 0.01$. $***p < 0.001$.

more clearly summarizes the dual indirect regulation of ISCA2 on ALAS2 expression. In brief, ROS accumulation is an indirect effect of ISCA2 depletion as well as a predisposing factor for increased IRP1 activity. Below, we will discuss the following aspects.

First, cell proliferation requires the production of large amounts of energy, the formation of macromolecule precursors and normal cellular metabolic pathways, as well as active mitochondrial function [22]. We demonstrated the importance of ISCA2 in maintaining normal cell proliferation through a series of experiments. We found that ISCA2 deficiency caused cell cycle disorder and induced G2/M phase arrest. ISCA2

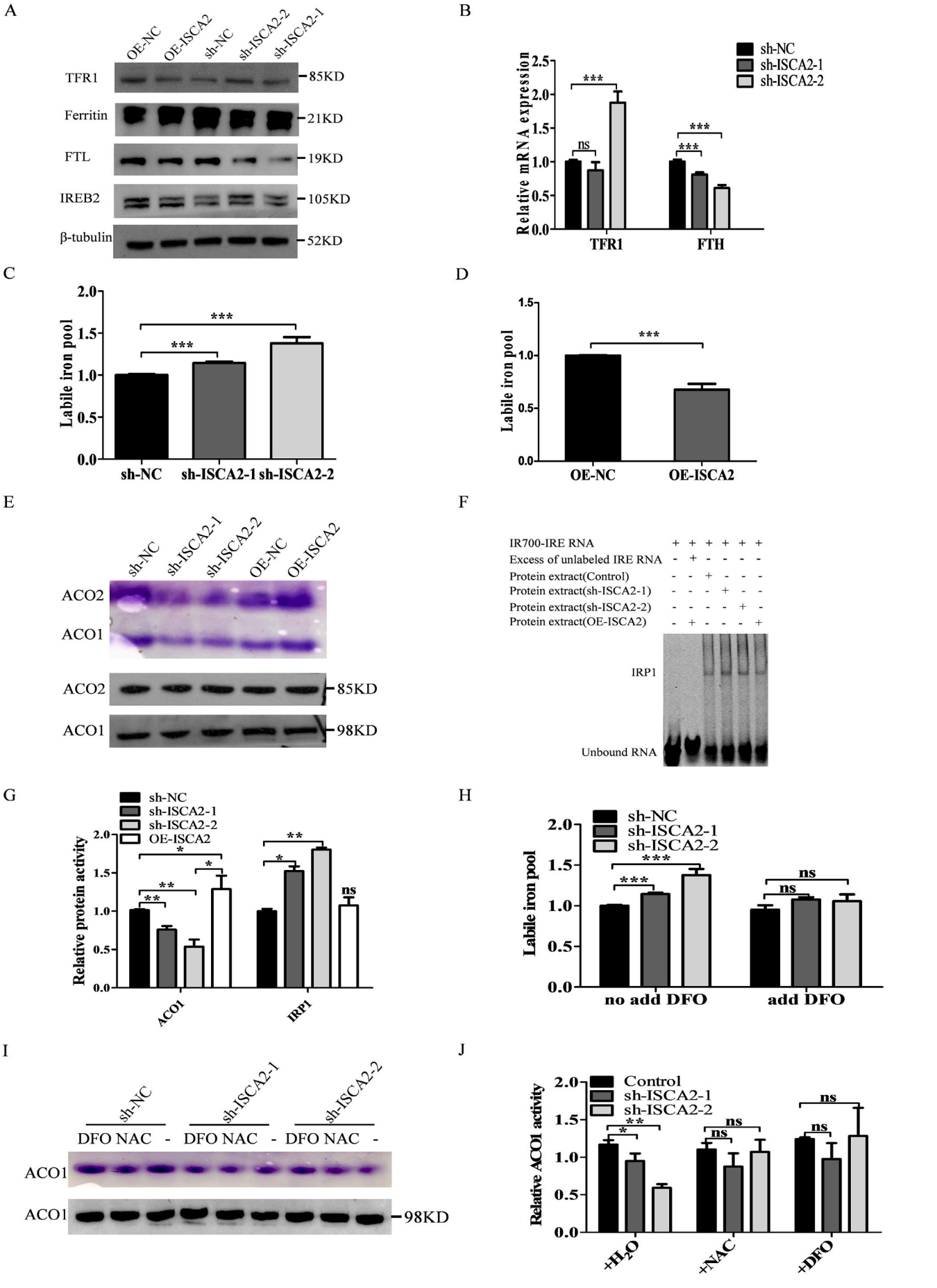

(caption on next page)

Fig. 7. Depletion of ISCA2 exerts complex effects on intracellular iron and leads to decreased ACO1 activity to further play the IRP1 function. (A) Expression of iron homeostasis proteins. (B) mRNA levels of transferrin and ferritin of low ISCA2 expressing cells were detected by qPCR. (C-D) Cytoplasmic labile iron pool in ISCA2 knockdown and ISCA2 overexpression K562 cells. (E) The activity of mitochondrial and cytoplasmic aconitase was analyzed by the in-gel activity assay. (F) An EMSA experiment based on near-infrared fluorescence was used to test the activity of IRP1. (G) Gray analysis and statistical results of Fig. 6E, F. (H) Cytoplasmic labile iron pool in cells with or without DFO. (I) The activity of c-aconitase after adding NAC and DFO was analyzed by the in-gel activity assay. (J) Gray analysis and statistical results of Fig. 6J. Images are representative of three independent experiments. Asterisks indicate that the differences between samples were statistically significant according to an independent-sample *t*-test, $*p < 0.05$, $**p < 0.01$. $***p < 0.001$.

is localized to the mitochondrial matrix, while proteins involved in cell cycle regulation are located in the nucleus [7,23–25]. A large number of reports on ISCA2 have not mentioned that ISCA2 deficiency affects the expression of cytoplasmic or nuclear proteins except ACO1. To determine whether cell cycle arrest is directly regulated by ISCA2, we examined the expression levels of proteins involved in cycle regulation. The results showed that when ISCA2 was deficient, the expression of CDK1 protein involved in G2/M phase regulation did not change significantly, and the expression of CyclinB protein slightly decreased, but the expression of proteins involved in G0/G1 and S phase regulation

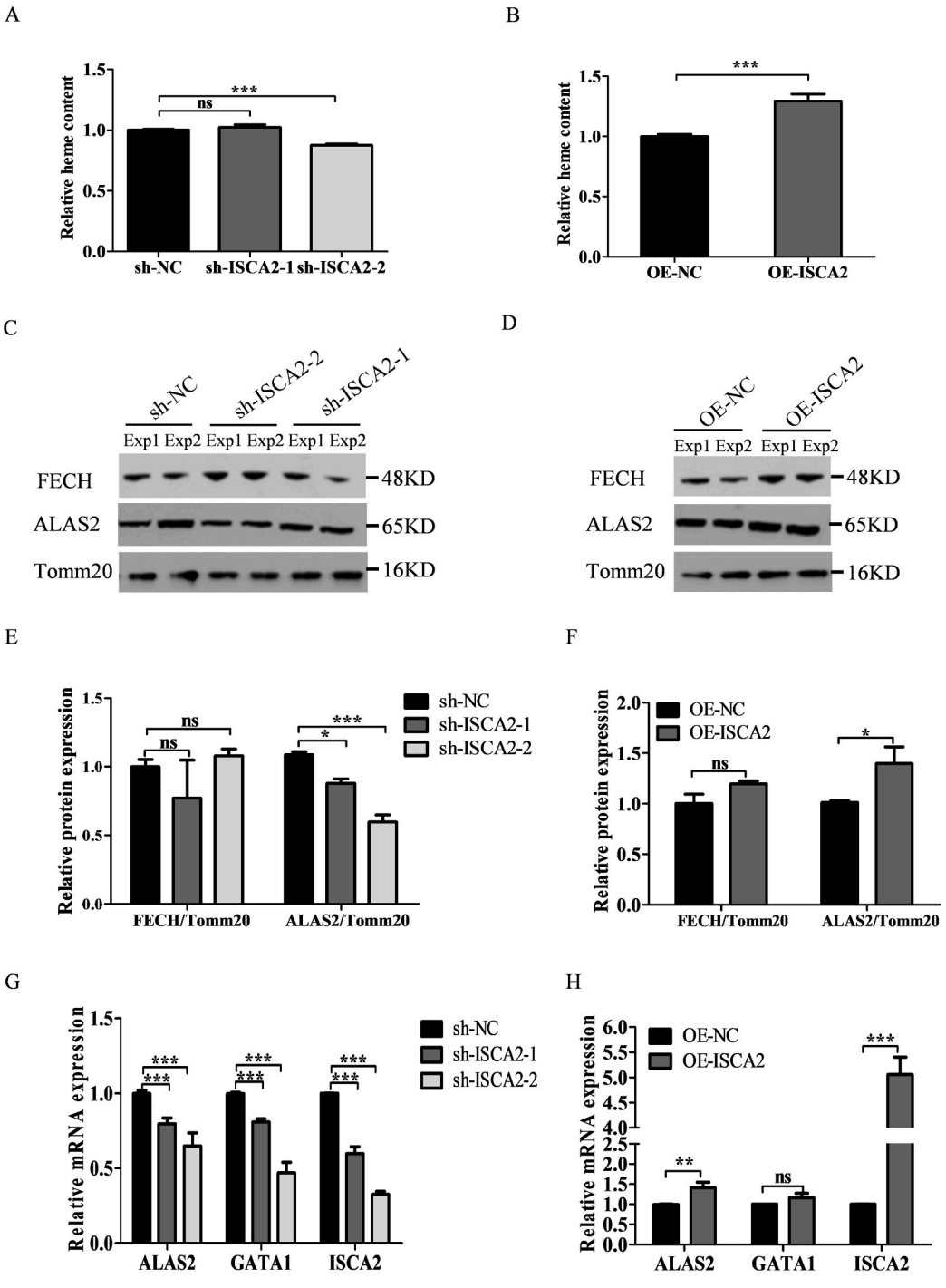

Fig. 8. ISCA2 affects the expression of ALAS2 by regulating the activity of ACO1 and IRPI, thus altering heme synthesis. (A-B) Measurement of cellular relative heme contents. (C-D) Expression levels of the major proteins involved in heme synthesis (ALAS2, FECH). (E–F) The relative protein expression levels of FECH and ALAS2 were analyzed according to the protein gray values. (G-H) The expression levels of genes related to heme synthesis mRNA by qPCR analysis. Images are representative of three independent experiments. Asterisks indicate that the differences between samples were statistically significant according to an independent sample *t*-test, $*p < 0.05$, $**p < 0.01$. $***p < 0.001$.

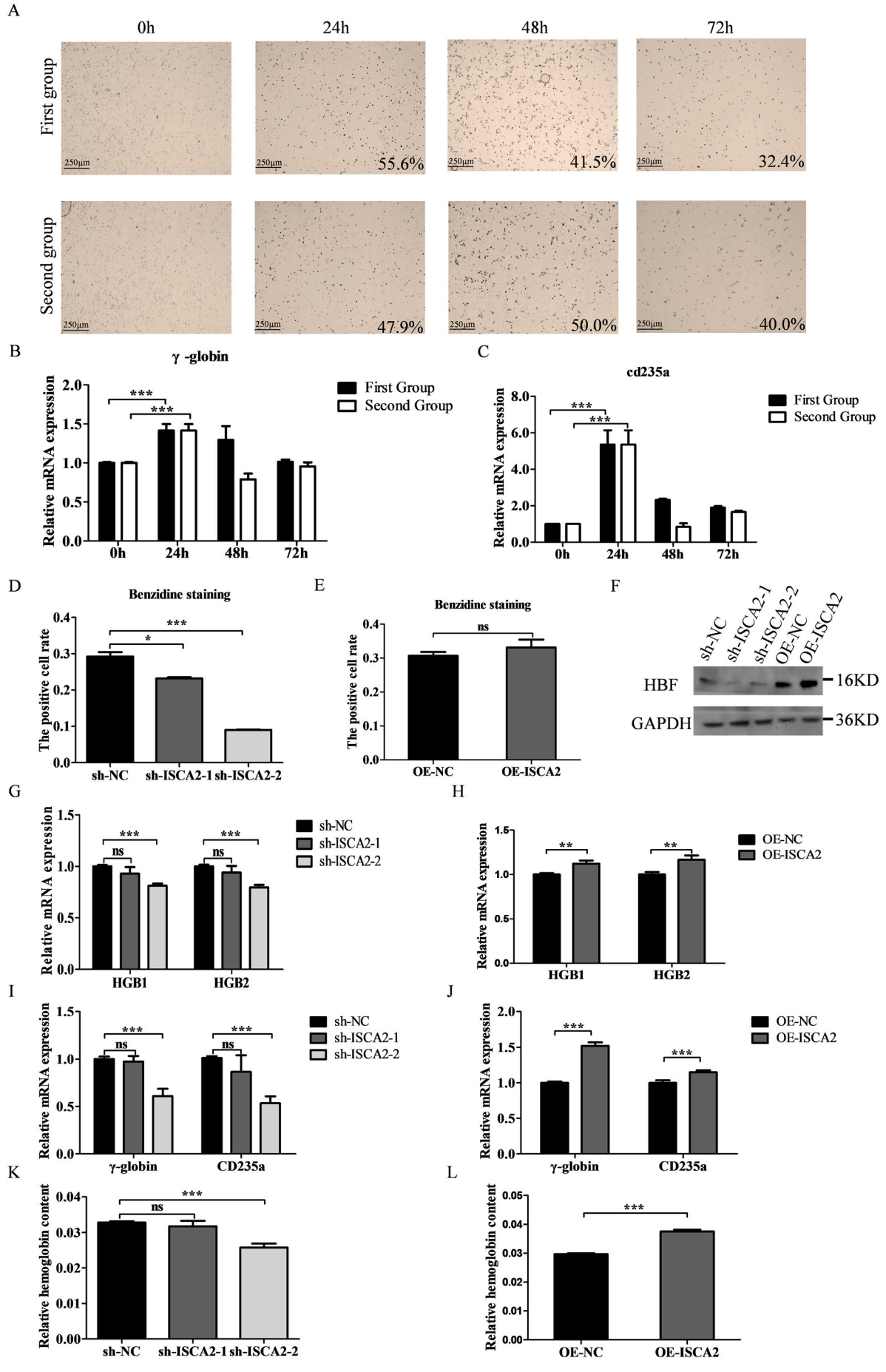

(caption on next page)

Fig. 9. ISCA2 knockdown repressed the erythroid differentiation of K562 cells, which was rescued by over-expressing ISCA2. (A) The fraction of benzidine-positive cells of wild-type k562 cells was determined by a benzidine-staining test. (B-C) Expression levels of genes related to erythroid differentiation mRNA of wild-type k562 by qPCR analysis. (D-E) The effects of knockdown and overexpression of ISCA2 on erythroid differentiation were determined by a benzidine-staining test. (F) Protein expressions of fetal hemoglobin detected by western blot in different cells. (G-J) qPCR analysis of critical genes concerned with erythroid differentiation in ISCA2 knockdown and high expression cells. (K-L) The relative heme content of cells was detected using a heme detection kit. Images are representative of three independent experiments. Asterisks indicate that the differences between samples were statistically significant according to an independent sample t-test, *p < 0.05, **p < 0.01. ***p < 0.001.

did not change significantly (Supplementary Fig. 1). Consistent with the results of cell cycle analysis, the decreased expression of CyclinB just indicated G2/M phase arrest, but there was no significant change in CDK1 expression. This may be due to the relatively stable expression of CDK1 throughout the cell cycle [26,27]. ROS can cause cell G2/M phase arrest has been demonstrated [28]. To determine whether ISCA2 deficiency indirectly regulates cyclin expression through ROS accumulation, we treated another group of cells with 5 mM NAC. We found that there was no significant difference in CyclinB expression in ISCA2 deficient cells compared with control cells when excessive intracellular ROS were removed. Therefore, we believe that G2/M phase arrest is an indirect phenotype caused by ROS accumulation in ISCA2 deficient cells. In addition, a large number of studies have shown that OXPHOS plays an important role in maintaining cell proliferation [29,30].This led us to wonder whether inhibition of cell proliferation by ISCA2 deficiency might be related to impaired OXPHOS.

ISCA2 plays an important role in the maturation of mitochondrial [4Fe-4S] proteins [31,32]. However, an article by Beilschmidt shows that ISCA2 is not required for the synthesis of [4Fe-4S] protein in mouse primary neurons and skeletal muscle cells, which is questionable because of the presence of severe leucoplasmic lesions in patients with ISCA2 mutations [8,10]. Hence, it seems likely that the insufficient depletion of ISCA2 mRNA by RNAi is a reasonable explanation for the lack of a phenotype in this study. There are >10 types of Fe-S proteins in mitochondria, and nearly 70% of Fe-S proteins are components of oxidative respiratory chain complexes [33]. NDUFS1 contains [2Fe-2S] and two [4Fe-4S] clusters, NDUFS8 carries two [4Fe-4S], SDHA and SDHB in complex II carry 3 Fe-S clusters ([2Fe-2S], [3Fe-4S], [4Fe-4S]),

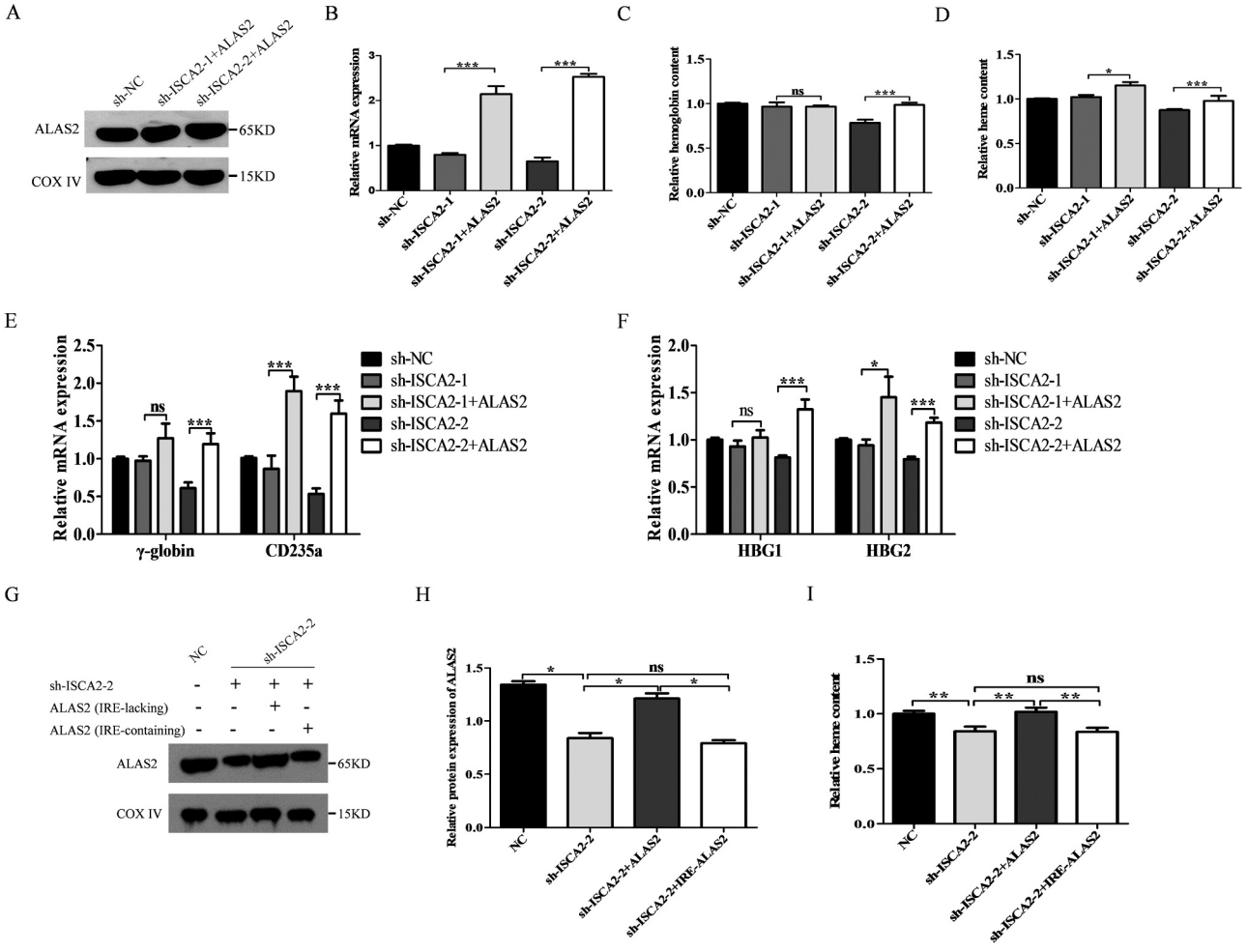

Fig. 10. Overexpression of ALAS2 in ISCA2 knockdown cells rescues erythroid differentiation. (A) Immunoblot showing the protein levels of the ALAS2 in K562 (ISCA2 knockdown/sh-NC) cells. (B) The mRNA expression levels of ALAS2 in K562 (ISCA2 knockdown/sh-NC) cells were also identified by quantitative real-time PCR. The relative mRNA expression using quantitative real-time PCR was normalized to GAPDH. (C) Measurement of cellular relative hemoglobin contents. (D) Measurement of cellular relative heme contents. (E-F) The expression levels of genes related to erythroid differentiation mRNA by qPCR analysis. Images are representative of three independent experiments. (G) Immunoblot showing the protein levels of the ALAS2. (H) Greyscale analysis of ALAS2 expression relative to COX IV. (I) Measurement of cellular relative heme contents. Asterisks indicate that the differences between samples were statistically significant according to an independent-sample t-test, *p < 0.05, **p < 0.01. ***p < 0.001.

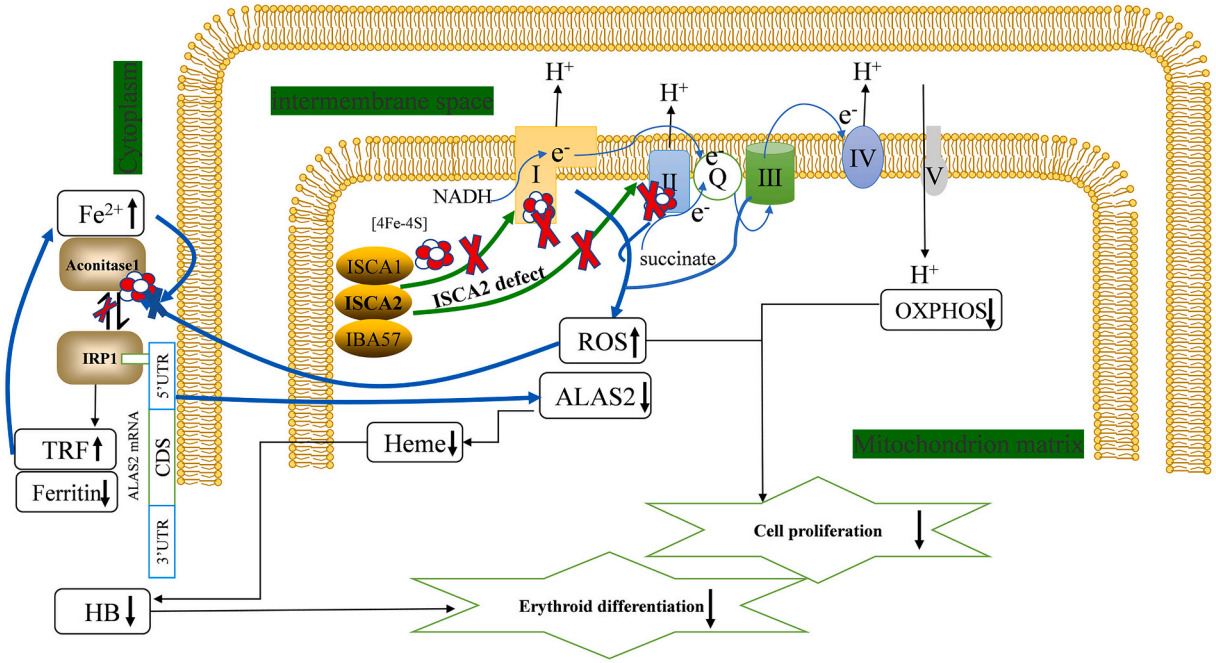

Fig. 11. Diagram of ISCA2 affecting cell proliferation and erythroid differentiation.

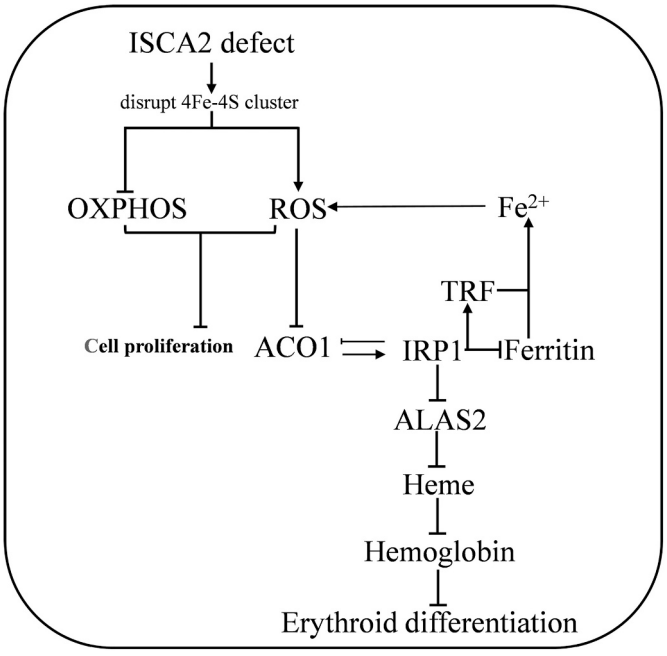

Fig. 12. Diagram of the double indirect regulation of ISCA2 on heme synthesis.

and the Rieske Fe-S protein (UQCRFS1) in complex III contains [2Fe-2S] [34–36]. Therefore, the subunit levels of complexes I and II containing [4Fe-4S] were significantly reduced by low ISCA2 expression, while the subunit levels of complexes IV and V containing no iron-sulfur clusters were unaffected. Additionally, our previous studies have shown that ISCA2 deficiency results in decreased activity of the respiratory chain complexes I, II, and III [37]. Interestingly, the expression level of complex III was also positively correlated with the expression level of ISCA2, but it contained the [2Fe-2S] cluster only. A possible explanation for this phenomenon is that defects in the synthesis of complexes I and II subunits lead to defects in the assembly of complexes I and II and their super complexes, and thus cause a chain reaction involving other complex members of the electron transport chain. In mammalian cells, mitochondrial OXPHOS is one of the main uses of iron. Iron-sulfur clusters and heme synthesis are the two main utilization pathways of iron, and multiple subunits of mitochondrial respiratory chain complex I–IV contain iron-sulfur clusters and heme [38,39]. Our study found that ISCA2 deficiency leads to disruption of cellular iron metabolism and reduced intracellular ferritin. Coincidentally, recent studies have shown that the mRNA-binding protein Tristetraprolin (TTP) is activated in response to iron deficiency to degrade the mRNA of proteins containing iron and sulfur clusters, especially the UQCRFS1 subunit of complex III and the NDUFS1 subunit of complex I [40]. This may also explain the decreased expression of UQCRFS1 and UQCRB.

The generation of ATP requires mitochondrial complexes I and II to transfer NADH and FADH2 from the TCA cycle to mitochondrial complex III, and mitochondrial complex IV reduces O2 and generates H2O [41]. We measured the total amount of ATP and lactic acid in the cell and used seahorse XFe96 extracellular flux analyzer to detect the energy metabolism of the cell. The experimental results showed that the decrease in ATP content and aerobic respiration capacity can be explained by our previous data. The increase in lactic acid level indicates cellular metabolism changes to glycolysis, but this change is not sufficient to maintain the level of ATP in cells. Therefore, further experiments are necessary to explore the specific transformation mechanism.

Mitochondrial complexes I and III are the main sources of intracellular ROS production, and complex II can also produce ROS [42,43]. A certain level of ROS is important to maintain the proliferation and signal transduction of tumor cells. However, in some tumor cells, high expression of ROS can induce cells in a state of oxidative stress, secondary cell damage, and genomic instability, and lead to cell apoptosis [44,45]. Our results suggest that ISCA2 can indirectly affect mitochondrial ROS production by influencing the function of the electron transport chain, and excessive ROS can induce apoptosis and even mitochondrial morphological destruction, which is an indirect phenotype of ISCA2. Previous studies have shown that enhanced mitochondrial biogenesis can promote the synthesis of iron-sulfur clusters [46], but whether there is no reverse regulatory effect is still being discussed. Our experiment preliminarily found that ISCA2 inhibits mitochondrial biogenesis only in the case of extreme depletion; the specific mechanism may be that it affects [4Fe-4S] protein synthesis, affects the

mitochondrial respiratory chain, and causes ROS accumulation, further aggravating mitochondrial damage.

Second, we unexpectedly found that ISCA2-deficient cells have reduced heme content and ISCA2 overexpressing cells have higher heme content than the control group, suggesting a role of ISCA2 in heme synthesis, contrary to previous studies in Hela cells [7]. We believe that the effect of ISCA2 on heme synthesis may be cell-specific, since erythroid cells need to synthesize large amounts of heme. For Hela cells, the heme content is low, so it is not easy to show significant content change. However, we must acknowledge that the effect of extreme ISCA2 depletion, with only a 10% to 15% reduction in heme content, is small. This may be related to ISCA2's dual and indirect regulation of heme synthesis. We found that the expression of ISCA2 can promote the synthesis of hemoglobin in erythroid cells. We speculate that ISCA2 regulates the synthesis of hemoglobin by regulating heme synthesis. Heme synthesis in human and animal cells requires eight enzymes. The first and last three enzymes in the synthesis pathway are located in the mitochondria, and the remaining four are located in the cytoplasm [39,47]. Heme synthesis can be directly regulated by the content of substrates and enzymes. As FECH is a [2Fe-2S] protein that is not affected by ISCA2, it is interesting that the protein and mRNA expression of ALAS2 decreased. But why does ISCA2 deficiency cause a decrease in ALAS2 expression?

ALAS2 is expressed only in erythroid cells such as K562 [39]. The expression of ALAS2 is regulated by IRP1. Two RNA-binding proteins IRP1 and IRP2 regulate iron metabolism by binding to the iron response element domain [48]. IRP1 can bind to the IRE on the 3′UTR of the transferrin receptor mRNA to stabilize its expression, and bind to the IRE on the 5′UTR of the ferritin or ALAS2 mRNA to inhibit its translation [49–51]. We proved that low expression of ISCA2 decreases cytoplasmic ACO1 activity. We investigated whether this translated to IRP1 activity using an EMSA assay. Elevated IRP1 activity inhibits ALAS2 translation, which may explain the decline in ALAS2 caused by ISCA2 deficiency. Moreover, IRE-containing ALAS2 plasmid was transferred into ISCA2-deficient cells, which did not rescue the expression of ALAS2 and the synthesis of heme, contrary to transfection IRE-containing ALAS2 plasmid. This further confirms that IRP1 binds IRE on the 5′UTR of ALAS2 to inhibit its translation, while ISCA2 regulates ALAS2 doubly and indirectly. As a bifunctional protein, IRP1 has a stronger ability to bind [4Fe-4S] clusters when there is sufficient intracellular iron, so it performs ACO1 activity, but the combination of excessive ferrous iron and ROS may lead to damage of the ACO1 cluster and higher IRP1 function. When intracellular iron is deficient, its IRE binding activity is stronger, playing the role of iron regulatory protein [52]. We conducted a preliminary study on iron metabolism and found that the expression of ferritin in ISCA2-deficient cells was significantly reduced, the expression of transferrin receptor was slightly increased, and the content of unstable iron pools in the cells increased. These findings indicate cellular iron deficiency and impaired iron usage. This can explain the decreased activity of ACO1 and increased activity of IRP1. Interestingly, the mRNA level of the erythroid transcription factor GATA1 also decreased. Coincidentally, a recent article pointed out that enhanced mitochondrial biogenesis in erythroid cells will upregulate the expression of GATA1, which will promote the expression of transferrin to counteract the inhibitory effect of iron-sulfur cluster synthesis on the expression of transferrin [46]. To verify whether the accumulation of ROS and iron divalent affects the activity of ACO1, we measured ACO1 in cells treated with NAC or DFO. The results showed that the accumulation of ROS and iron divalent is not beneficial to the normal activity of ACO1. We provided evidence that NAC and DFO can normalize ACO1 function as an aconitase, again showing that the effect of ISCA2 depletion on ACO1 function is indeed indirect and not a consequence of ISCA2 as a [4Fe-4S] cluster biosynthetic enzyme.

Indeed, it has been mentioned in the introduction that some ISC genes are very likely to have similar effects, such as IBA57 and ISCA1, have been reported in the literature to lead to anemia in zebrafish when these two genes are knocked out, which confirms their role in heme synthesis. However, the specific mechanism of anemia has not been further explored. As for ISCA2, this aspect has not been explored, so this is the reason why we explore the role and mechanism of ISCA2 in heme synthesis through erythroid cells. However, since we mainly study ISCA2, this paper mainly discusses the function of ISCA2. Next, we will explore the role and mechanism of other ISC genes in this aspect, and knock out ISCA2 in animals to further explore whether its defects can cause anemia in animals, which will make our research more meaningful.

In summary, our research shows that ISCA2 is a key protein necessary for mitochondrial [4Fe-4S] protein maturation, mitochondrial respiration, and participation in cellular iron homeostasis and erythroid hemoglobin synthesis.

4. Conclusion

This study aimed to explore the role of ISCA2 in the proliferation and differentiation of erythroid cells. This study and previous studies have demonstrated the role of ISCA2 as a mitochondrial targeted iron-sulfur cluster assembly protein in mitochondrial iron-sulfur cluster assembly and mitochondrial homeostasis. Using RNA interference to reduce the intracellular expression of ISCA2, we found that the proliferation of K562 cells was significantly inhibited and their ability to differentiate into erythrocytes was greatly reduced. Overexpression of ISCA2 rescued cell proliferation, while overexpression of ISCA2 or ALAS2 promoted erythroid lineage differentiation. We concluded that ISCA2 deficiency inhibits cell proliferation, which may be related to mitochondrial dysfunction, and regulates erythroid differentiation by regulating ALAS2 expression.

5. Materials and methods

5.1. Cell culture

The human erythroid leukemia K562 cell line (ATCC) was cultured in RPMI 1640 medium containing 20% fetal bovine serum (FBS) in an incubator at 37 °C and 5% CO2. 293T cells were grown in DMEM medium (10% FBS) in a 37 °C incubator with 5% CO2.

5.2. Plasmid construction

The short hairpin RNA sequences targeting ISCA2 and the empty vector were synthesized by GenScript (Nanjing, China). The sequences of short hairpin ISCA2 (sh-ISCA2–1, sh-ISCA2–2) were as follows: 5′-CCTCAGATTTAATCACTGGTT-3′, 5′-GCTCATTTCAAGTGTTGAACA-3′. The short hairpin RNA sequence was then cloned into the plasmid PLKO.1-EGFP (miaolingbio), which was used for lentivirus packaging, to obtain sh-ISCA2–1 and sh-ISCA2–2. The cDNA sequence of ISCA2 was acquired from NCBI GenBank (https://www.ncbi.nlm.nih.gov/) (Gene ID:122961). We synthesized ISCA2 cDNA at GenScript and cloned it into an overexpressed plasmid PlVX-cGFP-Puro, which was used for lentivirus packaging. The cDNA sequence of the overexpressed plasmid of IRE-lacking ALAS2 was obtained by querying the NCBI Gene Bank (Gene ID:212), synthesized by Beijing Tsingke, and cloned into the PlVX-cGFP-Puro plasmid. The cDNA sequence of the overexpressed plasmid of IRE-containing ALAS2 was also obtained by querying the NCBI Gene Bank (Gene ID:212), synthesized by Beijing Tsingke, and cloned into the PlVX-cGFP-Puro plasmid.

5.3. Lentiviral packaging and cell transfection

Lentiviral packaging was performed using 293 T cells. Briefly, 293 T cells were cultured in a six-well plate after they had reached 60%–70% confluence. The constructed sh-ISCA2–1, sh-ISCA2–2, OE-ISCA2, and OE-ALAS2 plasmids and empty vector (NC) were mixed with the

lentiviral packing auxiliary plasmids psPAX2 and PMD2.G (Addgene plasmid #12260 and #12259) at a ratio of 4:3:1, and the cells were co-transfected with lip3000 (Invitrogen, Shanghai, China) for viral packaging. The tar-get plasmid and two auxiliary plasmids called PSPAX2 and PMD2G were 2.5 μg and added in a ratio of 4:3:1. The supernatant was collected after 48 h and 72 h of culture. The virus supernatant was filtered with a 0.45 μm sterile filter, before concentrating with a lentivirus concentration reagent. The lentivirus titer was measured using a titer detection card (Biodragon, Beijing) before lentivirus transfection. Then, approximately 200,000 K562 cells were collected, and the volume of the required virus was calculated according to the multiplicity of infection (MOI) value of the K562 cells. At this point, the lentivirus and cells were mixed and cultured in serum-free medium for 12 h. Next, the complete medium was added for a further 12 h of culture, and then the medium was changed to complete medium. After adding the complete medium for 48 h of culture, GFP-positive cells were sorted by flow cytometry.

5.4. Western blotting

Total protein was extracted from harvested cells using RIPA cells lysis buffer (Beyotime, Shanghai), and quantified using a BCA™ Protein Assay Kit (Thermo Scientific). The following antibodies were used: AntiISCA2 (ab235776), Anti-ß tubulin (ab179511), Anti-GAPDH (ab181603), Anti-NDUFS1 (ab169540), Anti-NDUFS8 (ab170936), Anti-SDHA (ab137040), Anti-SDHB (ab175225), Anti-UQCRFS1 (ab191078), Anti-UQCRB (ab190360), Anti-COXIV (ab202554), Anti-ATP5A (ab176569), Anti-VDAC (ab14734), Anti-FECH (ab137042), Anti-ALAS2 (ab184964), Anti-HBF (ab137096), Anti-TFR1 (ab214039), Anti-Ferritin (ab75973), Anti-FTL (ab109373), Anti-IREB2 (ab181153), Anti-ACO1 (ab183721), and Anti-ACO2 (ab129069) (all Abcam), and Anti-IRP1 (sc-166,022, Santa Cruz). The secondary antibodies (e.g. Anti-rabbit IgG, Anti-mouse IgG) were purchased from Beyotime (Shanghai, China). ImageJ software was employed to perform grayscale analysis of the protein bands.

5.5. Total RNA extraction and quantitative real-time PCR

Total RNA was isolated from cells using RNAiso Plus (Takara, Beijing, China) according to the manufacturer's instructions. RNA was reverse transcribed into cDNA using the HiScript II RT SuperMix for qPCR (+gDNA wiper) kit (Vazyme, Nanjing, China). Real-time quantitative PCR of BioRad CFX was performed using SYBR Green (Vazyme, Nanjing, China) according to the manufacturer's instructions. The primer sequences used are shown in Table 1.

5.6. Cell growth analysis using CCK8

K562 cells were seeded in 96-well plates at a density of 2×10^3cells per well in 200 μL RPMI 1640 medium containing 20% FBS. When the cells were evenly spread to the bottom of the well, we added 20 μL CCK8 reagent and gently mixed. The plate was then placed in an incubator for 2 h and removed to measure the absorbance at 450 nm.

Table 1
Primers used in RT-QPCR experiment.

Primers	F-primer 5′-3′	R-primer 5′-3′
ISCA2	AGTTGCGTCCAGAGGCTTTT	CCCTTTCACGAAGGCCAAGC
ALAS2	TGTCCGTCTGGTGTAGTAATGA	GCTCAAGCTCCACATGAAACT
γ-globin	GCAGCTTGTCACAGTGCAGTT	TGGCAAGAAGGTGCTGACTTC
cd235a	GAGAAAGGGTACAACTTGCC	CATTGATCACTTGTCTCTGG
gata1	CCACACCACCACCACCACA	TCCTTCCCCTCCTCCTCTC
HBG1	GGAAGATGCTGGAGGAGAAACC	GTCAGCACCTTCTTGCCATGTG
HBG2	TGGACCCAGAGGTTCTTTGAC	AGGTGCTTTATGGCATCTCCC
FTH	TGAAGCTGCAGAACCAACGAGG	GCACACTCCATTGCATTCAGCC
TFRC	ATCGGTTGGTGCCACTGAATGG	ACAACAGTGGGCTGGCAGAAAC
GAPDH	CTGCCAACGTGTCAGTGGTG	TCAGTGTAGCCCAGGATGCC

5.7. Cell proliferation assay using the cell count technique

Cell counting experiments were also conducted in 96-well plates with 2×10^3cells/well in 200 μL of complete medium. Cells were counted at 0 h, 24 h, 48 h, 72 h, and 96 h, and the proliferation curve was plotted.

5.8. Colony formation assay

A total of 1×10^4 cells were collected from the positive transfection group and empty vector transfection group, and seeded into a semisolid culture medium containing 0.9% methylcellulose and 20% FBS. The cells were mixed in a 1 mL petri dish (35 mm in diameter) and incubated at 37 °C and 5% CO2 for 2 weeks. The colony formation rate was counted under an inverted microscope. A colony of >40 cells was considered as standard. Giemsa staining was also used to stain cell clones, and the clones were counted by eye.

5.9. Cell cycle analysis

The cell cycle staining kit (Beyotime, Shanghai, China) was used to detect the cell cycle distribution, strictly following the manufacturer's instructions. In brief, we first harvested the cells after synchronization treatment, cleaned the cells with PBS, and then fixed the cells with 70% ethanol for 12 h. The cells were washed again with PBS and stained with 100 μL RNase A at 37 °C for 30 min and 400 μL PI at 4 °C for 30 min. Finally, flow analysis was performed. The cell cycle data were analyzed by Flowjo software.

5.10. Cell apoptosis assay

The cell apoptosis staining kit (Bestbio, Shanghai, China) was used to detect early and late apoptotic cells. The suspended cells were harvested by centrifugation at 300–500 *g*, washed with precooled PBS, and resuspended in Annexin V 100 μL. Annexin V-PE 5 μL staining solution was added to the cell suspension and incubated avoiding light for 5 min. Next, 10 μL 7-AAD staining solution was added and incubated avoiding light for 3 min. Following incubation, 400 μL PBS was added and mixed gently, followed by flow cytometry detection. The early and late apoptotic cells were evaluated by Flowjo software.

5.11. Seahorse extracellular flux analysis

In brief, control group cells and experimental group K562 cells were tested on seahorse XFe96 extracellular flux analyzer. The seahorse XF Cell Energy Phenotype and Mito Stress Test kits were used according to the supplier's recommendation (Agilent). K562 cells were counted and seeded onto a 96-well cell culture plate pretreated with Cell-TAK (1206D69, Corning) on the day of the test as per the manufacturer's instructions. The optimal cell density of 2.5×10^4 cells per well, FCCP concentration of 2.0 μM, oligomycin concentration of 1.0 μM, and antimycin concentration of 1.0 μM were determined empirically. Each sample on each plate was repeated at least thrice, with three independent repetitions per plate. The oxygen consumption rate and extracellular acidification rate were quantified by wave software for seahorse.

5.12. Transmission electron microscopy

The samples were fixed overnight in 2.5% glutaraldehyde solution at 4 °C and then treated as follows: the stationary liquid was poured out and rinsed with phosphate buffer; the sample was fixed with 1% osmic acid for 1–2 h, rinsed again with phosphoric acid buffer, and then dehydrated with a gradient concentration of ethanol. The samples were then dehydrated with anhydrous ethanol before submerging in

anhydrous acetone. Osmosis, embedding, sectioning, staining, transmission electron microscopy, and photography was performed successively.

5.13. Mitochondrial DNA copy number

Genomic DNA was extracted from cells using Takara's Cell Genome Extraction Kit according to the manufacturer's instructions. The specific qPCR primers for mitochondrial DNA and nuclear DNA were designed to be detected by QPCR. The mitochondrial DNA copy number difference was calculated using the $2^{-\Delta\Delta T}$ relative quantitative method.

5.14. Mitochondrial biogenesis assays

Cells were stained with 100 nM Mitotracker Deep Red FM (Thermo Fisher, USA) and detected by flow cytometry. Data were analyzed using FlowJo7 software. Briefly, cells in the logarithmic growth phase were collected and incubated with dye for 30 min in a 37 °C incubator. The cells were then harvested and run on the flow cytometer. Data were derived from 10,000 cells and plotted as median fluorescence intensity.

5.15. Determination of mitochondrial ROS

ROS levels in mitochondria were measured using MitoSOX™ Red mitochondrial superoxide indicator. First, a 5 μM MitoSOX™ reagent working solution was prepared. Next, cells were stained for 30 min in a 37 °C incubator using a working solution. Following incubation, the cells were washed gently three times with warm buffer and the fluorescence was measured at $\lambda = 510$ nm (excitation) and $\lambda = 580$ nm (emission).

5.16. Ratio of NAD^+/NADH

The NAD^+/NADH ratio was determined using the NAD^+/NADH detection Kit (Beyotime, Shanghai, China). First, the working fluid was prepared according to the manufacturer's instructions. For suspension cells, 1 million cells were added to NAD/NADH extraction solution and gently blown to lyse cells. The cellular supernatant was collected after centrifugation at 12000 *g* for 10 min at 4 °C. Next, 50-100 μL of sample was collected and heated at 60 °C for 30 min to decompose NAD. The samples were then centrifuged at 10000 *g* for 5 min, and 20 μL of supernatant was collected and mixed 1:4.5 with working solution. The sample was coincubated for 10 min before adding 10 μL of color solution and continued to incubate for 30 min without light. Finally, the absorbance was measured at 450 nm. The relative quantification of NADH was achieved by correcting the results of cell BCA. The total amount of NAD and NADH was measured before heating at 60 °C. The amount of NAD was obtained by subtracting the amount of NADH, and then the ratio was obtained.

5.17. Labile iron pool (LIP) assay

Cells were collected and washed three times in serum-free medium. FerroOrange (0.5 μM) (Dojindo, Japan) was added to the cells with RPMI 1640 medium for 30 min at 37 °C, and the fluorescence intensity of each sample was detected by a microplate analyzer (Ex: 543 nm/ Em: 580 nm).

5.18. Visual detection of cis-aconitase activity

A nondenaturing gel with a thickness of 1.5 mm was prepared according to the following reagent concentration: Separation gel: 8% acrylamide, 132 mM Tris- HCl, 132 mM boric acid, 3.6 mM citric acid, 10% ammonium persulfate 10 μL/mL, TEMED 0.6 μL/mL; and concentrated gel: 4% acrylamide, 67 mM Tris-HCl, 67 mM boric acid, 3.6 mM citric acid, 10% ammonium persulfate 10 μL/mL, TEMED 1 μL/mL. The whole cells were lysed for 10 min at 4 °C using 1% Triton X-100 lysate (20 mM Tris-HCl, pH 8.0, 137 mM NaCl, 1% TritonX-100, 10% glycerin, 3 μM phenylmethanesulfonyl). The supernatant (containing the lysed protein component) was collected after centrifugation at 18000 *g* for 10 min at 4 °C. A BCA protein concentration assay kit was used to detect the protein concentration in supernatant components. Next, 100 μg protein was added to the corresponding volume of 5 × loading buffer (25-mM Tris-HCl pH 8.0, 10% glycerol, 0.025% bromophenol blue), and then the sample was added to each lane. Electrophoresis was performed at 200 V at 4 °C for 120 min. Following completion, the concentrated gel was cut down and incubated in a chromogenic substrate (100 mM Tris-HCl pH 8.0, 1 mM NADP+, 2.5 mM cis-Aconitum acid, 5 mM MgCl2, 1.2 mM MTT, 0.3 mM phenazinemethosulfate, and 5 U/mL Isocitrate dehydrogenase). Next, the gel was left shaking for either 2 h at 37 °C in the dark and analyzed by a gel imaging system.

5.19. Hemin colorimetric assay

A Hemin Colorimetric Assay Kit (Biovision, USA) was used to detect free hemin, according to the manufacturer's instructions. Briefly, 5×10^3–1×10^4 cells/well were used for each sample in a 96-well plate. The hemin production was measured at OD570.

5.20. Hemoglobin colorimetric assay

The total amount of intracellular hemoglobin was determined by the QuantiChrom™ Hemoglobin Assay Kit (DIHB-250) (BioAssay Systems, USA), in which the cell samples were assayed directly. Briefly, 50 μL of cell suspension was transferred into wells taking care to avoid bubble formation during the pipetting steps. Next, 200 μL reagent was added to the sample wells and tapped lightly to mix. The plate was then incubated for 5 min at room temperature before reading the OD at 390–405 nm (peak 400 nm).

5.21. Benzidine dyeing

The induced differentiated cells were collected and washed with PBS three times. Then, the cells were resuspended with 500 μL PBS and incubated with 14 μL 0.4% benzidine solution (benzidine powder dissolved in 1 mL 12% acetic acid) at room temperature for 3 min avoiding light. Next, 1 μL 30% H2O2 was added and allowed to incubate for 5 min, before adding 1 μL 5% sodium nitroferricyanide solution to the cells, mixing, and letting the mixture stand for 3 min. The benzidine positive cells were stained blue and the negative cells were not stained. The number of benzidine-positive cells in approximately 300–500 cells were counted and the percentage of positive cells was calculated.

5.22. Enzymatic activities and IRP1-binding activities

IRP1 binding activities were determined using a special RNA EMSA kit (SIDET001, ViageneBiotech, Changzhou, China) according to the manufacturer's instructions. Cell proteins were extracted using protein extraction kit (Viagene Biotech, Changzhou, China). Briefly, 15 μg proteins were added to a final volume of 10 μL in REMSA buffer at room temperature for 20 min. Following incubation, infrared fluorophore labeled probes (IR dye-labeled probe) were added and coincubated at room temperature for 20 min. The probe sequence was 5′-IR700-UCCUGCUUCAACAGUGCUUGGAC-GGAAC-3′. The gel was then prepared according to the instructions. The sample pre-pared in the previous step was mixed with 6 × loading buffer for gel electrophoresis on ice at 180 V until bromophenol blue reached the lower end of the gel. Finally, the gels were imaged with a LI-COR infrared imager (Odyssey).

Funding

This work was supported by grants of the National Natural Science

Foundation of China (Grant Number: 81671124, 31870775, 32170044).

CRediT authorship contribution statement

Jing Wang: Conceptualization, Methodology, Software, Validation, Investigation, Writing – original draft. **Mengyao Jiang:** Methodology, Formal analysis, Writing – review & editing. **Guanru Yue:** Validation, Investigation. **Lifei Zhu:** Data curation, Visualization. **Xueqing Wang:** Investigation, Visualization. **Mengxiang Liang:** Investigation, Visualization. **Xiaolin Wu:** Validation, Investigation. **Beibei Li:** Investigation, Visualization. **Yilin Pang:** Writing – review & editing, Visualization. **Guoqiang Tan:** Resources, Funding acquisition, Conceptualization, Supervision, Project administration. **Jianghui Li:** Funding acquisition.

Declaration of competing interest

The authors declare that they have no known competing financial interests or personal relationships that could have appeared to influence the work reported in this paper.

Acknowledgments

This investigation was supported by grants from the National Natural Science Foundation of China (81671124, 31870775, 32170044).

We appreciate the Scientific Research Center of Wenzhou Medical University for the service and technical support.

Appendix A. Supplementary data

Supplementary data to this article can be found online at https://doi.org/10.1016/j.bbamcr.2022.119307.

References

[1] R. Malkin, J.C. Rabinowitz, The reconstitution of clostridial ferredoxin, Biochem. Biophys. Res. Commun. 23 (1966) 822–827.
[2] J.W. Peters, J.B. Broderick, Emerging paradigms for complex iron-sulfur cofactor assembly and insertion, Annu. Rev. Biochem. 81 (2012) 429–450.
[3] R. Lill, V. Srinivasan, U. Mühlenhoff, The role of mitochondria in cytosolic-nuclear iron–sulfur protein biogenesis and in cellular iron regulation, Curr. Opin. Microbiol. 22 (2014) 111–119.
[4] C. Wachnowsky, I. Fidai, J.A. Cowan, Iron–sulfur cluster biosynthesis and trafficking – impact on human disease conditions, Metallomics 10 (2018) 9–29.
[5] S.A. Freibert, A.V. Goldberg, C. Hacker, S. Molik, P. Dean, T.A. Williams, S. Nakjang, S. Long, K. Sendra, E. Bill, et al., Evolutionary conservation and in vitro reconstitution of microsporidian iron-sulfur cluster biosynthesis, Nat. Commun. 8 (2017) 13932.
[6] R. Lill, S.A. Freibert, Mechanisms of mitochondrial iron-sulfur protein biogenesis, Annu. Rev. Biochem. 89 (2020) 471–499.
[7] A.D. Sheftel, C. Wilbrecht, O. Stehling, B. Niggemeyer, H.P. Elsasser, U. Muhlenhoff, R. Lill, The human mitochondrial ISCA1, ISCA2, and IBA57 proteins are required for [4Fe-4S] protein maturation, Mol. Biol. Cell 23 (2012) 1157–1166.
[8] L.K. Beilschmidt, S. Ollagnier de Choudens, M. Fournier, I. Sanakis, M.-A. Hograindleur, M. Clémancey, G. Blondin, S. Schmucker, A. Eisenmann, A. Weiss, et al., ISCA1 is essential for mitochondrial Fe4S4 biogenesis in vivo. Nature, Communications 8 (2017).
[9] M. Alfadhel, Multiple mitochondrial dysfunctions syndrome 4 due to ISCA2 gene defects: a review, Child. Neurol. Open 6 (2019) (2329048X19847377).
[10] Z.N. Al-Hassnan, M. Al-Dosary, M. Alfadhel, E.A. Faqeih, M. Alsagob, R. Kenana, R. Almass, O.S. Al-Harazi, H. Al-Hindi, O.I. Malibari, et al., ISCA2 mutation causes infantile neurodegenerative mitochondrial disorder, J. Med. Genet. 52 (2015) 186–194.
[11] J.T. Alaimo, A. Besse, C.L. Alston, K. Pang, V. Appadurai, M. Samanta, P. Smpokou, R. McFarland, R.W. Taylor, P.E. Bonnen, Loss-of-function mutations in ISCA2 disrupt 4Fe-4S cluster machinery and cause a fatal leukodystrophy with hyperglycinemia and mtDNA depletion, Hum. Mutat. 39 (2018) 537–549.
[12] D.P. Barupala, S.P. Dzul, P.J. Riggs-Gelasco, T.L. Stemmler, Synthesis, delivery and regulation of eukaryotic heme and Fe-S cluster cofactors, Arch. Biochem. Biophys. 592 (2016) 60–75.
[13] F.V. Mello, M.G.P. Land, E.S. Costa, C. Teodósio, M.-L. Sanchez, P. Bárcena, R. T. Peres, C.E. Pedreira, L.R. Alves, A. Orfao, Maturation-associated gene expression profiles during normal human bone marrow erythropoiesis, Cell Death Dis. (2019) 5.
[14] R. Nilsson, I.J. Schultz, E.L. Pierce, K.A. Soltis, A. Naranuntarat, D.M. Ward, J. M. Baughman, P.N. Paradkar, P.D. Kingsley, V.C. Culotta, et al., Discovery of genes essential for heme biosynthesis through large-scale gene expression analysis, Cell Metab. 10 (2009) 119–130.
[15] U. Mühlenhoff, N. Richter, O. Pines, A.J. Pierik, R. Lill, Specialized function of yeast Isa1 and Isa2 proteins in the maturation of mitochondrial [4Fe-4S] proteins, J. Biol. Chem. 286 (2011) 41205–41216.
[16] J.C. Waller, S. Alvarez, V. Naponelli, A. Lara-Nuñez, I.K. Blaby, V. Da Silva, M. J. Ziemak, T.J. Vickers, S.M. Beverley, A.S. Edison, et al., A role for tetrahydrofolates in the metabolism of iron-sulfur clusters in all domains of life, Proc. Natl. Acad. Sci. U. S. A. 107 (2010) 10412–10417.
[17] L. Mosconi, A. Pupi, M.J. De Leon, Brain glucose hypometabolism and oxidative stress in preclinical Alzheimer's disease, Ann. N. Y. Acad. Sci. 1147 (2008) 180–195.
[18] C. Xie, J. Yi, J. Lu, M. Nie, M. Huang, J. Rong, Z. Zhu, J. Chen, X. Zhou, B. Li, et al., N-acetylcysteine reduces ROS-mediated oxidative DNA damage and PI3K/Akt pathway activation induced by Helicobacter pylori infection, Oxidative Med. Cell. Longev. 2018 (2018) 1874985.
[19] L.K. Beilschmidt, S. Ollagnier de Choudens, M. Fournier, I. Sanakis, M. A. Hograindleur, M. Clémancey, G. Blondin, S. Schmucker, A. Eisenmann, A. Weiss, et al., ISCA1 is essential for mitochondrial Fe(4)S(4) biogenesis in vivo, Nat. Commun. 8 (2017) 15124.
[20] A. Jain, A. Singh, N. Maio, T.A. Rouault, Assembly of the [4Fe-4S] cluster of NFU1 requires the coordinated donation of two [2Fe-2S] clusters from the scaffold proteins, ISCU2 and ISCA1, Hum. Mol. Genet. 29 (2020) 3165–3182.
[21] D. Suraci, G. Saudino, V. Nasta, S. Ciofi-Baffoni, L. Banci, ISCA1 orchestrates ISCA2 and NFU1 in the maturation of human mitochondrial [4Fe-4S] proteins, J. Mol. Biol. 433 (2021), 166924.
[22] H. Ni, M. Guo, X. Zhang, L. Jiang, S. Tan, J. Yuan, H. Cui, Y. Min, J. Zhang, S. Schlisio, et al., VEGFR2 inhibition hampers breast cancer cell proliferation via enhanced mitochondrial biogenesis, Cancer Biol. Med. 18 (2021) 139–154.
[23] O. Afanzar, G.K. Buss, T. Stearns, J.E. Ferrell Jr., The nucleus serves as the pacemaker for the cell cycle, eLife 9 (2020).
[24] W.A. Bresnahan, I. Boldogh, T. Ma, T. Albrecht, E.A. Thompson, Cyclin E/Cdk2 activity is controlled by different mechanisms in the G0 and G1 phases of the cell cycle, Cell Growth Diff. 7 (1996) 1283–1290.
[25] N. Davezac, V. Baldin, B. Gabrielli, A. Forrest, N. Theis-Febvre, M. Yashida, B. Ducommun, Regulation of CDC25B phosphatases subcellular localization, Oncogene 19 (2000) 2179–2185.
[26] M. Castedo, J.L. Perfettini, T. Roumier, G. Kroemer, Cyclin-dependent kinase-1: linking apoptosis to cell cycle and mitotic catastrophe, Cell Death Differ. 9 (2002) 1287–1293.
[27] M.B. Kastan, J. Bartek, Cell-cycle checkpoints and cancer, Nature 432 (2004) 316–323.
[28] Y.H. Choi, Isorhamnetin induces ROS-dependent cycle arrest at G2/M phase and apoptosis in human hepatocarcinoma Hep3B cells, Gen. Physiol. Biophys. 38 (2019) 473–484.
[29] P. Ghosh, C. Vidal, S. Dey, L. Zhang, Mitochondria targeting as an effective strategy for cancer therapy, Int. J. Mol. Sci. 21 (2020).
[30] Y. Guo, X. Chi, Y. Wang, B.C. Heng, Y. Wei, X. Zhang, H. Zhao, Y. Yin, X. Deng, Mitochondria transfer enhances proliferation, migration, and osteogenic differentiation of bone marrow mesenchymal stem cell and promotes bone defect healing, Stem Cell Res Ther 11 (2020) 245.
[31] D. Brancaccio, A. Gallo, M. Mikolajczyk, K. Zovo, P. Palumaa, E. Novellino, M. Piccioli, S. Ciofi-Baffoni, L. Banci, Formation of [4Fe-4S] clusters in the mitochondrial iron-sulfur cluster assembly machinery, J. Am. Chem. Soc. 136 (2014) 16240–16250.
[32] D. Chiabrando, F. Bertino, E. Tolosano, Hereditary ataxia: a focus on heme metabolism and Fe-S cluster biogenesis, Int. J. Mol. Sci. 21 (2020).
[33] K. Fiedorczuk, J.A. Letts, G. Degliesposti, K. Kaszuba, M. Skehel, L.A. Sazanov, Atomic structure of the entire mammalian mitochondrial complex I, Nature 538 (2016) 406–410.
[34] N. Maio, K.S. Kim, A. Singh, T.A. Rouault, A single adaptable cochaperone-scaffold complex delivers nascent iron-sulfur clusters to mammalian respiratory chain complexes I-III, Cell Metab. 25 (945-953) (2017), e946.
[35] L.A. Sazanov, P. Hinchliffe, Structure of the hydrophilic domain of respiratory complex I from Thermus thermophilus, Science (New York N.Y.) 311 (2006) 1430–1436.
[36] D.A. Stroud, E.E. Surgenor, L.E. Formosa, B. Reljic, A.E. Frazier, M.G. Dibley, L. D. Osellame, T. Stait, T.H. Beilharz, D.R. Thorburn, et al., Accessory subunits are integral for assembly and function of human mitochondrial complex I, Nature 538 (2016) 123–126.
[37] Y. Ling, L. Ruolan, N. Huan, H. Li, L. Yanchun, W. Weilong, L. Jianghui, T. Guoqiang, L. Jianxin, Elucidation of roles of protein ISCA2 in the control of mitochondrial function, Chinese J. Cell Biol. (2018).
[38] J. Gao, Q. Zhou, D. Wu, L. Chen, Mitochondrial iron metabolism and its role in diseases, Clin. Chim. Acta 513 (2021) 6–12.
[39] S.A. Swenson, C.M. Moore, J.R. Marcero, A.E. Medlock, A.R. Reddi, O. Khalimonchuk, From synthesis to utilization: the ins and outs of mitochondrial heme, Cells 9 (2020).
[40] T. Sato, H.-C. Chang, M. Bayeva, J.S. Shapiro, L. Ramos-Alonso, H. Kouzu, X. Jiang, T. Liu, S. Yar, K.T. Sawicki, et al., mRNA-binding protein tristetraprolin is essential for cardiac response to iron deficiency by regulating mitochondrial function, Proc. Natl. Acad. Sci. 115 (2018) E6291–E6300.
[41] P. Licznerski, H.A. Park, H. Rolyan, R. Chen, N. Mnatsakanyan, P. Miranda, M. Graham, J. Wu, N. Cruz-Reyes, N. Mehta, et al., ATP synthase c-subunit leak causes aberrant cellular metabolism in fragile X syndrome, Cell 182 (2020) 1170–1185.e1179.

[42] P. Hernansanz-Agustin, J.A. Enriquez, Generation of reactive oxygen species by mitochondria, Antioxidants (Basel) (2021) 10.
[43] Y. Ni, C. Eng, Vitamin E protects against lipid peroxidation and rescues tumorigenic phenotypes in cowden/cowden-like patient-derived lymphoblast cells with germline SDHx variants, Clin. Cancer Res. 18 (2012) 4954–4961.
[44] T. Finkel, From sulfenylation to sulfhydration: what a thiolate needs to tolerate, Sci. Signal. 5 (2012) pe10.
[45] E. Panieri, M.M. Santoro, ROS homeostasis and metabolism: a dangerous liason in cancer cells, Cell Death Dis. 7 (2016), e2253.
[46] P. La, J.H. Oved, V. Ghiaccio, S. Rivella, Mitochondria biogenesis modulates iron–sulfur cluster synthesis to increase cellular iron uptake, DNA Cell Biol. 39 (2020) 756–765.
[47] M.D. Maines, A. Kappas, Metals as regulators of heme metabolism, Science (New York N.Y.) 198 (1977) 1215–1221.
[48] M.W. Hentze, M.U. Muckenthaler, B. Galy, C. Camaschella, Two to tango: regulation of Mammalian iron metabolism, Cell 142 (2010) 24–38.
[49] J. Kato, M. Kobune, S. Ohkubo, K. Fujikawa, M. Tanaka, R. Takimoto, K. Takada, D. Takahari, Y. Kawano, Y. Kohgo, et al., Iron/IRP-1-dependent regulation of mRNA expression for transferrin receptor, DMT1 and ferritin during human erythroid differentiation, Exp. Hematol. 35 (2007) 879–887.
[50] M. Muckenthaler, N.K. Gray, M.W. Hentze, IRP-1 binding to ferritin mRNA prevents the recruitment of the small ribosomal subunit by the cap-binding complex eIF4F, Mol. Cell 2 (1998) 383–388.
[51] M. Sanchez, B. Galy, B. Schwanhaeusser, J. Blake, T. Bähr-Ivacevic, V. Benes, M. Selbach, M.U. Muckenthaler, M.W. Hentze, Iron regulatory protein-1 and -2: transcriptome-wide definition of binding mRNAs and shaping of the cellular proteome by iron regulatory proteins, Blood 118 (2011) e168–e179.
[52] T.A. Rouault, N. Maio, Biogenesis and functions of mammalian iron-sulfur proteins in the regulation of iron homeostasis and pivotal metabolic pathways, J. Biol. Chem. 292 (2017) 12744–12753.